

ARTICLE

ATM inhibition drives metabolic adaptation via induction of macropinocytosis

Zhentai Huang^{1*}, Chi-Wei Chen^{1*}, Raquel Buj¹, Naveen Kumar Tangudu¹, Richard S. Fang¹, Kelly E. Leon^{1,2}, Erika S. Dahl², Erika L. Varner³, Eliana von Krusenstiern³, Aidan R. Cole¹, Nathaniel W. Snyder³, and Katherine M. Aird¹

Macropinocytosis is a nonspecific endocytic process that may enhance cancer cell survival under nutrient-poor conditions. Ataxia-Telangiectasia mutated (ATM) is a tumor suppressor that has been previously shown to play a role in cellular metabolic reprogramming. We report that the suppression of ATM increases macropinocytosis to promote cancer cell survival in nutrient-poor conditions. Combined inhibition of ATM and macropinocytosis suppressed proliferation and induced cell death both in vitro and in vivo. Supplementation of ATM-inhibited cells with amino acids, branched-chain amino acids (BCAAs) in particular, abrogated macropinocytosis. Analysis of ATM-inhibited cells in vitro demonstrated increased BCAA uptake, and metabolomics of ascites and interstitial fluid from tumors indicated decreased BCAAs in the microenvironment of ATM-inhibited tumors. These data reveal a novel basis of ATM-mediated tumor suppression whereby loss of ATM stimulates protumorigenic uptake of nutrients in part via macropinocytosis to promote cancer cell survival and reveal a potential metabolic vulnerability of ATM-inhibited cells.

Introduction

Macropinocytosis is a nonselective endocytic process whereby cells take up fluid, macromolecules, metabolites, and other cargo from the surrounding microenvironment (King and Kay, 2019; Palm, 2019; Zhang and Comisso, 2019). Many studies have evaluated the critical role of macropinocytosis as a nutrient-scavenging mechanism in cancers under nutrient-deprived conditions (Comisso et al., 2013; Davidson et al., 2017; Hodakoski et al., 2019; Kamphorst et al., 2015; Kim et al., 2018; Lee et al., 2019; Redelman-Sidi et al., 2018; Tejada-Munoz et al., 2019; Yao et al., 2019). These studies have mainly focused on cancers with high PI3K activity, such as those with mutant RAS or phosphatase and tensin homolog (PTEN) loss, which act upstream of the Rac1-Pak1 actin remodeling pathway to promote macropinosome formation (Zhang and Comisso, 2019). Recent studies suggest that the signaling to promote macropinocytosis, which merges at the activation of Rac1, is more complex (Hobbs and Der, 2022), and other tumor-associated pathways, such as HIF1 and NRF2, have recently been shown to promote macropinocytosis (Su et al., 2021; Zhang et al., 2022). One central nutrient-sensing pathway that is linked to macropinocytosis is the mTORC1 pathway (Palm, 2022). mTORC1 is a master regulator of cell growth, proliferation, and macromolecule synthesis

(Kim and Guan, 2019; Saxton and Sabatini, 2017). mTORC1 activity is regulated at many levels, including an abundance of the branched-chain amino acids (BCAAs) leucine and isoleucine (Foster and Fingar, 2010). Studies have shown that the down-regulation of mTORC1 promotes macropinocytosis (Dai et al., 2021; Dendo et al., 2018; Sung et al., 2015). This would presumably restore energy homeostasis through the uptake of free amino acids, extracellular proteins, or other nutrients.

Ataxia-Telangiectasia mutated (ATM) is a tumor suppressor, and mutation or loss of ATM expression promotes genomic instability and predisposes cells to tumorigenesis (McKinnon, 2004, 2012). While ATM is important for the response to DNA double-strand breaks (Shiloh, 2003), it is also known to play a role in cellular metabolism (Dahl and Aird, 2017; Guleria and Chandna, 2016). We previously demonstrated that ATM is wild type, and its signaling is upregulated in ovarian cancer (Chen et al., 2020). We also found that ATM expression is inversely correlated with metabolic gene signatures in ovarian cancer patient specimens. Furthermore, we and others have shown that the inhibition of ATM increases the uptake of glucose and glutamine to provide nutrients for cell growth and proliferation (Aird et al., 2015; Dahl and Aird, 2017). Our previous results

¹Department of Pharmacology & Chemical Biology and UPMC Hillman Cancer Center, University of Pittsburgh School of Medicine, Pittsburgh, PA; ²Biomedical Sciences Graduate Program, Penn State College of Medicine, Hershey, PA; ³Center for Metabolic Disease Research, Department of Cardiovascular Sciences, Temple University, Philadelphia, PA.

*Zhentai Huang and Chi-Wei Chen contributed equally to this paper. Correspondence to Katherine M. Aird: kaa140@pitt.edu.

© 2022 Huang et al. This article is distributed under the terms of an Attribution-Noncommercial-Share Alike-No Mirror Sites license for the first six months after the publication date (see <http://www.rupress.org/terms/>). After six months it is available under a Creative Commons License (Attribution-Noncommercial-Share Alike 4.0 International license, as described at <https://creativecommons.org/licenses/by-nc-sa/4.0/>).

suggest that inhibition of ATM reprograms metabolism through the suppression of p53 signaling and enhanced c-MYC protein stability (Aird et al., 2015). Indeed, these and other models where ATM suppression or mutation has been shown to alter cellular metabolism are in cells with WT p53 and normal c-MYC expression. Whether ATM similarly alters nutrient uptake and cellular metabolism in the context of cancers with mutated p53 and high c-MYC expression is unclear. Moreover, ATM inhibitors are currently undergoing clinical trials (Jin and Oh, 2019), although they are not generally effective as a monotherapy (Batey et al., 2013; Chen et al., 2020; Fujimaki et al., 2012; Golding et al., 2012; Jin and Oh, 2019; Riches et al., 2020). Thus, understanding how the inhibition of ATM drives metabolic reprogramming may be important toward identifying potential resistance mechanisms or other targets that could be used in combination with these inhibitors in ATM-WT tumors.

Here, we found that the suppression of ATM increases nutrient uptake in p53 mutated and c-MYC-amplified cancer cells even upon a single knockdown of key transporters. This nonspecific nutrient uptake under nutrient-poor conditions occurred in part via macropinocytosis. Underscoring the importance of this pathway in ATM-inhibited cells, suppression of macropinocytosis significantly inhibited the proliferation of cancer cells both in vitro and in vivo. Analysis of metabolites suggested increased uptake of BCAAs in ATM-inhibited tumors and cells, and supplementing cells in vitro with exogenous BCAAs decreased macropinocytosis. Together, these data demonstrate that inhibition of ATM reprograms cellular metabolism in part via induction of macropinocytosis and reveal that macropinocytosis is a vulnerability of ATM-inhibited tumors.

Results and discussion

Inhibition of ATM kinase activity increases glucose and glutamine consumption in a transporter-independent mechanism

ATM loss or inhibition alters whole-body and cellular metabolism (Aird et al., 2015; Cosentino et al., 2011; Dahl and Aird, 2017; Guleria and Chandna, 2016; Valentin-Vega et al., 2012). We previously published that an increased uptake and consumption of glucose and glutamine, two carbon sources that are critically important for cancer cell metabolism, is in part due to the inactivation of p53 and increased c-MYC stability downstream of ATM knockdown (Aird et al., 2015). However, the transporter-dependence of nutrient uptake in ATM-inhibited cells has never been directly tested. To answer this question, we used three ovarian cancer cell lines with functional/WT ATM and differential status of p53 and c-MYC (Ovcar8: mutant p53, c-MYC amplification; Ovcar3: mutant p53; Ovcar10: het mutant p53) and tested glucose and glutamine uptake upon inhibition of ATM in nutrient-limiting conditions. These conditions were chosen as replete media often masks metabolism-mediated effects and does not faithfully recapitulate the nutrients observed in tumors in vivo (Cantor, 2019). Ovarian cancers have activated ATM signaling, and therefore, inhibition of ATM is being explored as a therapeutic strategy in these and other solid tumors (Chen et al., 2020; Jin and Oh, 2019; Weber and Ryan, 2015). We

found that pharmacological inhibition of ATM kinase activity using two different small-molecule inhibitors (KU60019 and AZD0156), both of which decrease Chk2 phosphorylation (Fig. 1 A and Fig. S1 A), increased glucose and glutamine consumption in the ovarian cancer cell lines regardless of p53 or c-MYC status (Fig. 1, B and C; and Fig. S1, B–D). Interestingly, knockdown of the glucose transporters SLC2A1/GLUT1 and SLC2A4/GLUT4 or the glutamine transporter SLC1A5/ACST2 did not respectively alter the glucose or glutamine uptake induced by ATM inhibition (Fig. 1, D–G), although knockdown did suppress uptake of metabolites in parental cells (Fig. S1, E and F). Although compensation through other transporters is possible, these data suggest another mechanism may also be contributing to metabolite uptake in these cells.

Inhibition of ATM kinase activity induces macropinocytosis

Previous studies have shown that macropinocytosis is one mechanism whereby cancer cells scavenge nutrients from the microenvironment to support survival and proliferation under nutrient-poor conditions (Commisso et al., 2013; Davidson et al., 2017; Hodakoski et al., 2019; Kamphorst et al., 2015; Kim et al., 2018; Lambies and Commisso, 2022; Lee et al., 2019; Palm, 2019; Palm et al., 2017; Recouvreur and Commisso, 2017; Redelman-Sidi et al., 2018; Yao et al., 2019; Zhang and Commisso, 2019). Macropinocytosed nutrients are transported within the macropinosome to the lysosome where the engulfed macromolecules may be degraded (King and Kay, 2019; Palm, 2019) and released into the cytoplasm by specific permeases on the lysosome membrane (Perera and Zoncu, 2016), which are different than the cell-surface-bound transporters. In nutrient-limiting conditions, 24 h of cotreatment of cells with the ATM inhibitor and 5-(N-ethyl-N-isopropyl)-amiloride (EIPA), a Na⁺/H⁺ exchanger that is an inhibitor of macropinocytosis (Commisso et al., 2014; Ivanov, 2008), decreased consumption of glucose and glutamine (Fig. S2 A). Therefore, we aimed to confirm these results using a fluorescently labeled 70 kD dextran. Due to its large size, 70-kD dextran is used as a surrogate for macropinocytosis as it cannot be taken up through other endocytic pathways (Commisso et al., 2014; Ivanov, 2008). While the inhibition of ATM in complete media did not increase dextran uptake after 2 h treatment, we did observe an increase under starvation (basal media) conditions (Fig. 2, A–D; gating strategy Fig. S2 B; media conditions detailed in Materials and methods). This medium was chosen because we reasoned that limiting extracellular metabolites may help to promote the macropinocytosis process. Other nutrient-limiting media had a similar effect (Fig. S2 C). A different ATM inhibitor and ATM knockdown using shRNA also increased dextran uptake (Fig. S2, D–F). To address the possibility that FITC fluorescence may be affected by low pH when macropinosomes fuse with lysosomes (Chen et al., 2008), we performed a time course experiment. A significant increase in dextran uptake was observed starting as early as 15 min with a peak at 1 h (Fig. S2 G). While the signal is still high at 90 min and 2 h, we do start to see a decrease, suggesting quenching of FITC within the lysosome. We also observed an increase in tetramethylrhodamine (TMR)-labeled 70-kD dextran, whose fluorescence is not quenched by low pH (Fig. S2 H). Ataxia

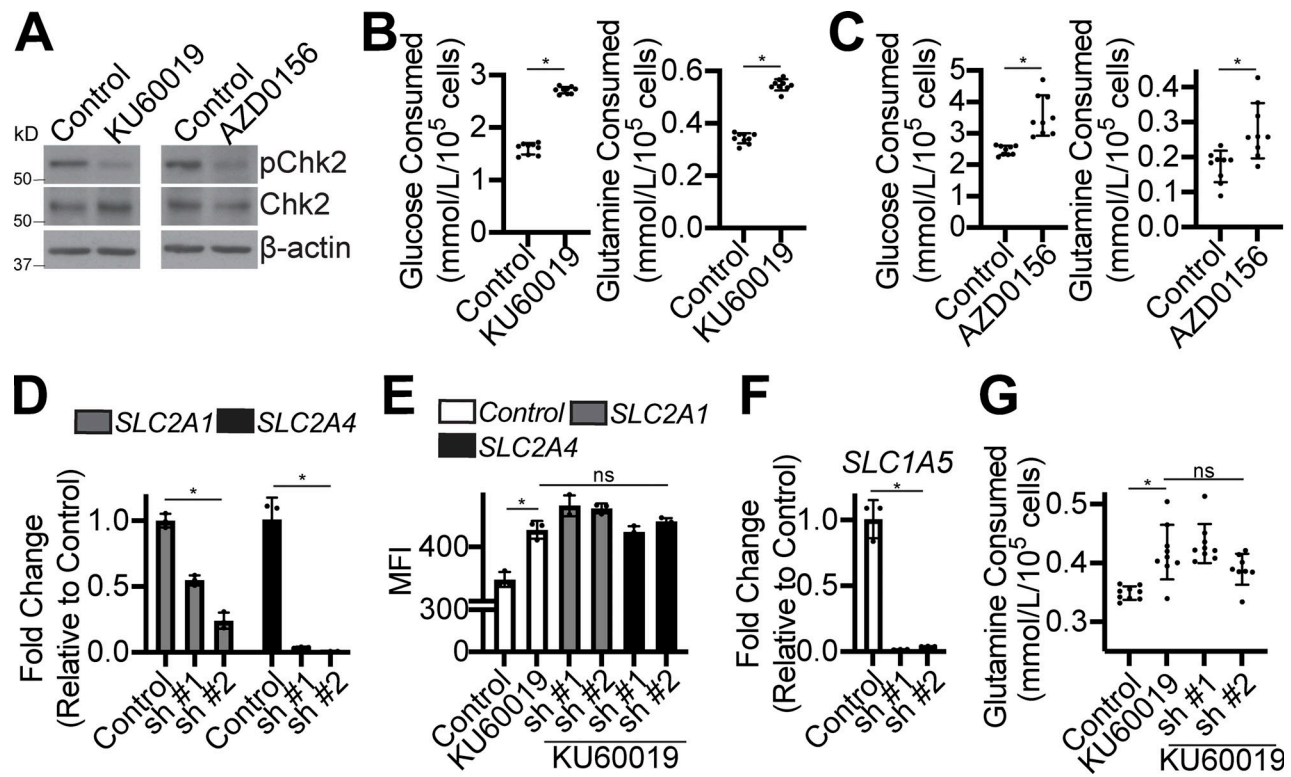


Figure 1. Inhibition of ATM increases glucose and glutamine consumption, while knockdown of glucose or glutamine transporters in ATM-inhibited cells has no effect. (A–C) Ovarc8 cells were treated with the ATM inhibitors (10 μ M KU60019 or 1 μ M AZD0156) for 24 h in RPMI-1640 + 0.1% FBS. (A) pChk2 and total Chk2 expression were determined by immunoblotting. β -actin was used as a loading control. One of three experiments is shown. (B and C) Glucose and glutamine uptake were determined. $n = 9$ /group, one of three experiments is shown. Data represent mean \pm SD. * $P < 0.005$; unpaired two-sided t test. (D) Ovarc3 cells were infected with lentivirus expressing short hairpin RNAs (shRNAs) targeting *SLC2A1* (GLUT1) or *SLC2A4* (GLUT4). shGFP was used as a control. mRNA expression was determined by RT-qPCR. $n = 3$ /group, one of two experiments is shown. Data represent mean \pm SD. * $P < 0.01$ vs. control; one-way ANOVA. (E) Same as D, but cells were treated with 10 μ M KU60019 for 24 h in RPMI-1640 + 0.1% FBS, and glucose uptake using the fluorescent glucose analog 2NBDG was determined by flow cytometry. MFI = median fluorescence intensity. $n = 3$ /group, one of three experiments is shown. Data represent mean \pm SD. * $P < 0.0001$ vs. KU60019; ns = not significant; one-way ANOVA with Tukey’s multiple comparisons. (F) Ovarc8 cells were infected with lentivirus expressing short hairpin RNAs (shRNAs) targeting *SLC1A5*. shGFP was used as a control. mRNA expression was determined by RT-qPCR. $n = 3$ /group, one of two experiments is shown. Data represent mean \pm SD. * $P < 0.0001$ vs. control; one-way ANOVA. (G) Same as F, but cells were treated with 10 μ M KU60019 for 24 h in RPMI-1640 + 0.1% FBS, and glutamine uptake was determined. $n = 9$ /group, one of three experiments is shown. Data represent mean \pm SD. * $P < 0.005$ vs. KU60019; ns = not significant; one-way ANOVA with Tukey’s multiple comparisons.

telangiectasia and Rad3-related protein (ATR) is another kinase that is associated with the DNA damage response and has similar and often overlapping roles with ATM (Shiloh, 2003). Inhibition or knockdown of ATR did not increase dextran uptake, suggesting this is specific for ATM (Fig. S2, I–L). This is consistent with our previous report demonstrating that the knockdown of ATM, but not ATR, rescues proliferation defects due to metabolic deficiencies (Aird et al., 2015).

To further confirm that the increase in dextran uptake is due to macropinocytosis, we cotreated cells with EIPA. Treatment of cells with EIPA suppressed the ATM-mediated increase in dextran uptake (Fig. 2, A–D). EIPA in combination with the ATM inhibitor did not increase pChk2 (Fig. S2 M), suggesting that the decrease in macropinocytosis is not the result of increased ATM activity. EIPA alone decreased pChk2, although to varying degrees in the cell lines tested. These data indicate that the signaling downstream of ATM to regulate macropinocytosis is likely not through Chk2, and pChk2 is only a surrogate for confirming the activity of the ATM inhibitors. Macropinosome

formation requires Rac1 activity for actin remodeling and membrane ruffling (Fujii et al., 2013), and the inhibition of Rac1 using eHop-016 also decreased dextran uptake (Fig. 2 B). Together, these data indicate that suppression of ATM induces macropinocytosis.

Suppression of macropinocytosis limits survival only in ATM-inhibited cells

We next aimed to determine whether macropinocytosis is required for the survival of ATM-inhibited cells. We treated cells with the ATM inhibitor KU60019 and inhibited macropinocytosis using EIPA. The combination decreased proliferation and increased apoptosis compared with single-treatment controls in multiple cell lines (Fig. 3, A and B; and Fig. S3, A and B). Analysis of proliferation data shows modest synergy (Fig. S3 C). These experiments were performed in replete media, which modestly increases dextran uptake after a chronic 3-d exposure to the ATM inhibitor that is inhibited by EIPA (Fig. S3 D; media conditions detailed in Materials and methods). Modest synergy

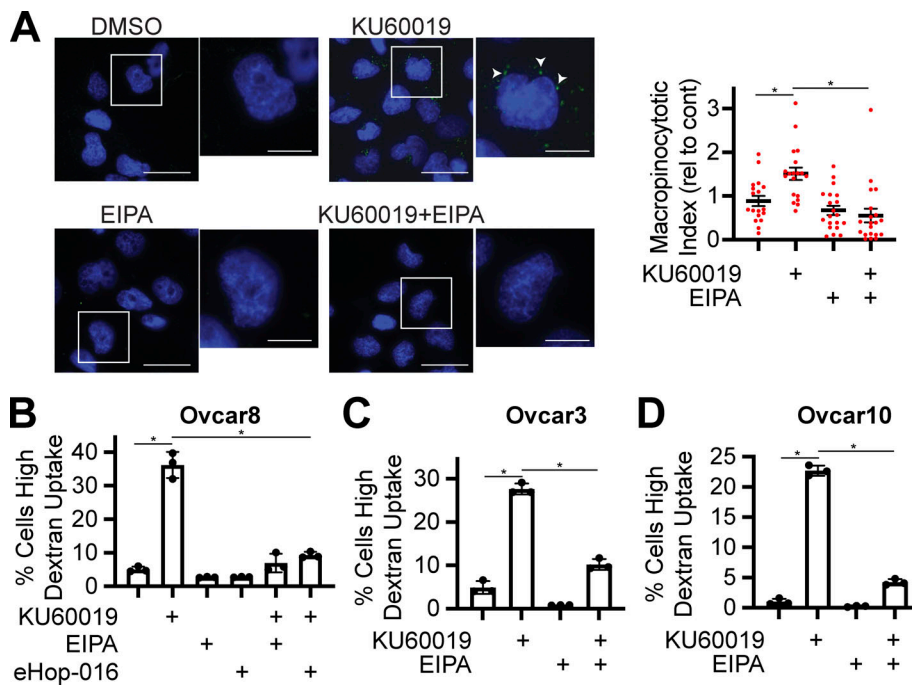


Figure 2. Inhibition of ATM kinase activity induces macropinocytosis. (A) Ovar8 cells were treated with the ATM inhibitor 10 μ M KU60019 for 2 h in basal media, and 70 kD dextran uptake was determined by fluorescence microscopy. Scale bars = 25 μ m (large images), 15 μ m (insets). Arrowheads point to dextran-FITC. N > 20/group, one of three experiments is shown. Data represent mean \pm SD. *P < 0.005 vs. KU60019; one-way ANOVA with Tukey's multiple comparisons. (B) Ovar8 cells were treated with the ATM inhibitor KU60019 (10 μ M) alone or in combination with the macropinocytosis inhibitor EIPA (25 μ M) or eHop-016 (2.5 μ M) for 2 h in basal media, and dextran uptake was determined by flow cytometry. n = 3/group, one of at least four experiments is shown. (C and D) Ovar3 (C) and Ovar10 (D) cells were treated with the ATM inhibitor KU60019 (10 μ M) alone or in combination with the macropinocytosis inhibitor EIPA (25 μ M) for 2 h in basal media, and dextran uptake was determined by flow cytometry. n = 3/group, one of at least three experiments is shown. Data represent mean \pm SD. *P < 0.0001 vs. KU60019; one-way ANOVA with Tukey's multiple comparisons.

was also observed using nutrient-limiting media (Fig. S3 E). Inhibition of Rac1 using eHop-016 also decreased proliferation in combination with the ATM inhibitor in multiple media (Fig. S3, F and G). The same concentration of EIPA did not affect the proliferation of nonmacropinocytotic normal fibroblasts (Fig. S3 H). In in vivo experiments, the synergy between the ATM inhibitor and EIPA was more pronounced (Fig. 3, C-E). The combination also induced apoptosis as we observed increased cleaved caspase 3 staining by immunohistochemistry (IHC) in the tumors (Fig. 3, F and G). We also validated that KU60019 inhibited ATM by blotting for pChk2 in the tumors (Fig. 3 H and Fig. S3 I). Similar to our in vitro studies, we noted that pChk2 was decreased in the EIPA-alone treated mice. To confirm whether the inhibition of ATM induces macropinocytosis in vivo, mice were injected with fluorescently labeled 70-kD dextran 30 min prior to harvesting the tumor. Consistent with our in vitro data (Fig. 2), KU60019 induced macropinocytosis, which was suppressed by EIPA (Fig. 3, I and J). Together, these data demonstrate that inhibition of macropinocytosis limits proliferation/survival only of cells where ATM is inhibited.

Macropinocytosis induced by ATM inhibition increases BCAA uptake and affects mTORC1 activity

Next, we aimed to determine the metabolic consequences of increased macropinocytosis due to the inhibition of ATM. Previous studies have demonstrated that diverse nutrients including proteins, lipids, glucose, amino acids, and others are taken up by macropinocytosis to promote cancer cell survival under nutrient stress (Commisso et al., 2013; Hodakoski et al., 2019; Kamphorst et al., 2015; Kim et al., 2018; Lee et al., 2019; Palm, 2019; Palm et al., 2017; Recouvreux and Commisso, 2017; Redelman-Sidi et al., 2018; Tejada-Munoz et al., 2019; Zhang and Commisso, 2019). Thus, we reasoned that metabolites needed to

support survival in ATM-inhibited cells would suppress macropinocytosis. Toward this goal, we supplemented cells in basal media with a variety of nutrients. Supplementation with amino acids, but not with glucose, glutamine, or pyruvate, decreased the ATM inhibitor-mediated dextran uptake (Fig. 4 A). While nonessential amino acids (NEAAs) did not affect dextran uptake, supplementation of BCAAs partially but significantly decreased dextran uptake (Fig. 4 B), although we cannot rule out increased uptake via transporters that then suppress macropinocytosis. To better assess whether BCAAs are taken up by macropinocytosis, we used isotope-labeled BCAAs and observed an increase in labeled valine and (iso)leucine in ATM-inhibited cells (Fig. 4 C). Intracellular BCAA abundance was also increased in this condition (Fig. S4 A), supporting the interpretation that the observed increase in labeling is not due to a decrease in the intracellular BCAA pool size (Fig. S4 B). Using publicly available datasets from cell lines (depmap.org), we found protein expression of ATM or pChk2 negatively correlated with the abundance of BCAAs (Fig. 4 D and Fig. S4 C), suggesting that this is a more general phenomenon of ATM low cells. BCAAs can either be catabolized into alpha ketoacids for downstream metabolic processes or directly affect mTORC1 (in the case of leucine/isoleucine) and protein synthesis (Sivanand and Vander Heiden, 2020). While we did not observe marked differences in alpha ketoacids (KMV/KIC or KIV) in ATM-inhibited cells (Fig. S4 D), inhibition of ATM decreased phosphorylation of S6K and 4EBP1 (Fig. 4, E and F), although to a different extent in the cell lines tested. These data suggest a decrease in mTORC1 activity. There was also a positive correlation between phosphorylation of ATM pathway activation and mTORC1 pathway activation in ovarian cancer patient samples from The Cancer Genome Atlas (TCGA; Fig. S4 E). In vitro, supplementation of BCAAs rescued the ATM inhibitor-mediated decrease in mTORC1 activity (Fig. 4

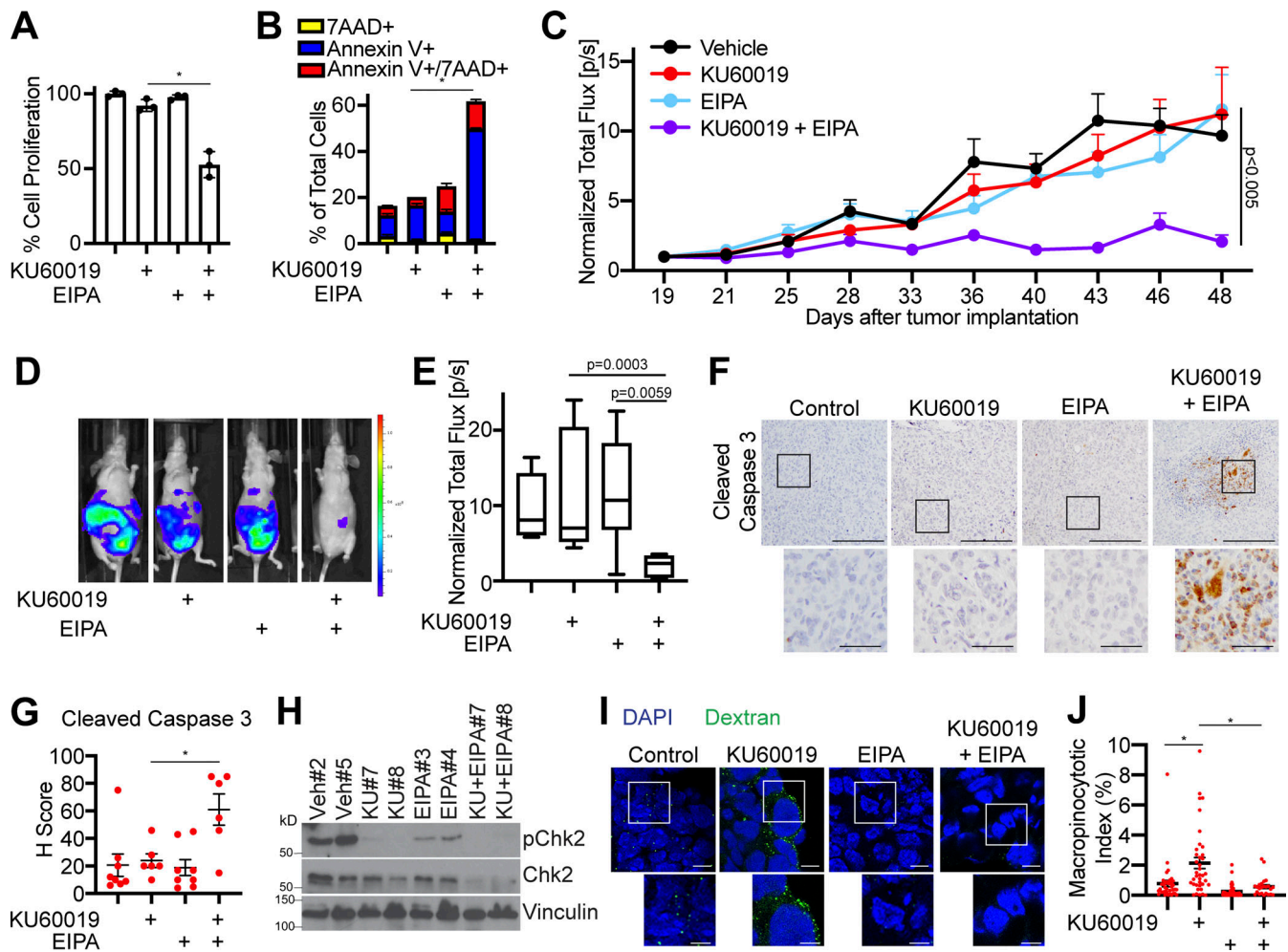


Figure 3. Inhibition of macropinocytosis is a vulnerability of ATM-inhibited cells both in vitro and in vivo. (A and B) Ovarc8 cells were treated with the ATM inhibitor KU60019 (2 μ M) or the macropinocytosis inhibitor EIPA (2 μ M) alone or in combination for 3 d in RPMI-1640 + 5% FBS. **(A)** Proliferation was assessed by crystal violet staining. $n = 3$ /group, one of three experiments is shown. Data represent mean \pm SD. * $P < 0.001$; one-way ANOVA. **(B)** Apoptosis was assessed by Annexin V/7AAD staining. $n = 3$ /group, one of three experiments is shown. Data represent mean \pm SD. * $P < 0.001$; one-way ANOVA. **(C)** Ovarc8 cells expressing luciferase were injected intraperitoneally into nude mice (6–8 mice/group). At day 19, mice were randomized and thereafter treated daily through intraperitoneal injection with the ATM inhibitor KU60019 (10 mg/kg) or the macropinocytosis inhibitor EIPA (10 mg/kg) alone and in combination. Bioluminescence flux was determined using noninvasive IVIS imaging. Shown is the tumor growth curve over 30 d normalized to Day 19 tumors. Longitudinal analysis: combination vs. vehicle, $P = 0.00141$; combination vs. KU60019, $P = 0.002334$; combination vs. EIPA, $P = 0.003603$; linear mixed model fit REML. **(D)** Representative luciferase images of mice from each group at Day 48. **(E)** Quantification of D normalized to Day 19 tumors. Cross-sectional analysis: ANOVA with Wilcoxon rank sum test. **(F)** Representative cleaved caspase 3 immunohistochemistry in the indicated tumors. Scale bars = 100 μ m (large images), 25 μ m (insets). **(G)** H-Score of cleaved caspase 3 IHC. Data represent mean \pm SEM. * $P < 0.01$; one-way ANOVA. **(H)** Representative pChk2 and total Chk2 immunoblot analysis of the indicated tumors. Vinculin was used as a loading control. **(I)** Representative confocal images of dextran-FITC in the indicated tumors. Scale bars = 10 μ m (large images), 2.5 μ m (insets). **(J)** Macropinocytotic index of dextran-FITC uptake in the tumors was assessed. Data represent mean \pm SEM. * $P < 0.0005$ vs. KU60019; one-way ANOVA with Tukey's multiple comparisons.

E) and slightly rescued the decrease in proliferation in combined ATM inhibitor and macropinocytosis inhibitor-treated cells (Fig. S4 F). These data are consistent with previous literature demonstrating that inhibition of mTORC1 activity upregulates macropinocytosis (Dendo et al., 2018; Sung et al., 2015). In contrast, other studies have shown that mTORC1 is activated by macropinocytosis (Meng et al., 2022; Pacitto et al., 2017; Yoshida et al., 2015), or mTORC1 controls the balance between extracellular protein scavenging, catabolism in the lysosome, and protein translation rates (Nofal et al., 2017; Palm et al., 2015). The discrepancy in these observations may be due to media

conditions and an acute vs. chronic response. In our studies, mTORC1 was decreased in the acute setting in nutrient-limiting conditions where few extracellular metabolites are available to be consumed. The addition of BCAAs rescued the suppression of mTORC1 activity in this acute setting. It is possible that a more chronic exposure of cells to ATM inhibitors may in fact increase mTORC1 through the enhanced uptake of BCAAs. Furthermore, exactly how ATM inhibition is decreasing mTORC1 activity in these cells remains to be determined. Previous studies have linked ATM signaling upstream of mTORC1 to both positively and negatively regulating its activity (Alexander et al., 2010;

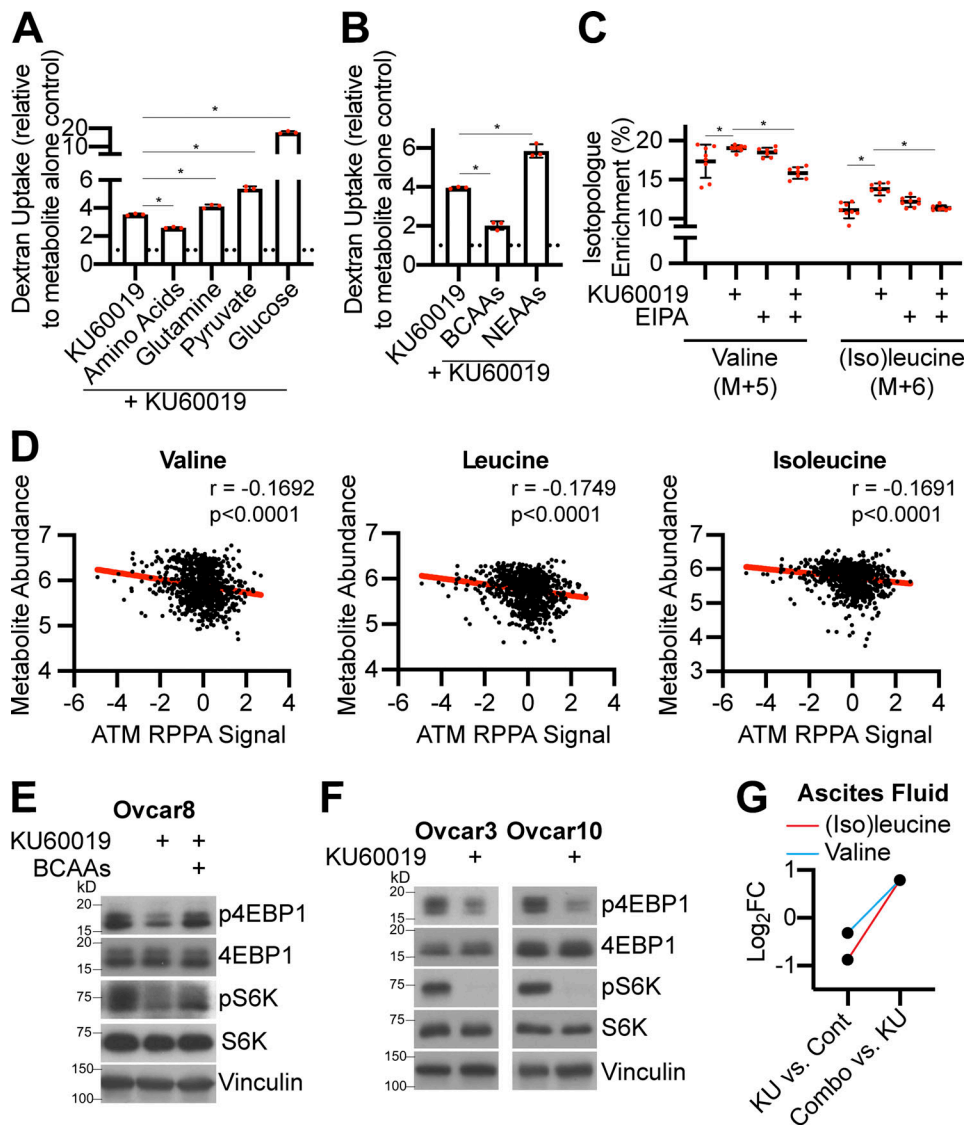


Figure 4. ATM inhibitor-induced macropinocytosis leads to increased branched-chain amino acid uptake and affects mTORC1 activity. (A and B) Ovar8 cells were treated with the ATM inhibitor KU60019 (10 μ M) alone or in combination with the indicated metabolites (concentrations in Materials and Methods) for 2 h in basal media, and dextran uptake was determined by flow cytometry. $n = 3$ /group, one of at least three experiments is shown. Data represent mean \pm SD. Dotted line indicates controls for each metabolite. * $P < 0.05$ vs. KU60019; one-way ANOVA with Tukey's multiple comparisons. **(C)** Ovar8 cells were treated with the ATM inhibitor KU60019 (10 μ M) alone or in combination with the macropinocytosis inhibitor EIPA (25 μ M) for 2 h in basal media, and isotopologue enrichment of BCAAs was assessed by mass spectrometry. $n = 3$ /group, one of at least three experiments is shown. Data represent mean \pm SD. * $P < 0.05$ vs. KU60019; one-way ANOVA with Tukey's multiple comparisons. **(D)** BCAA metabolite abundance vs. ATM protein expression from DepMap.org. **(E)** Ovar8 cells were treated with the ATM inhibitor KU60019 (10 μ M) alone or in combination with 200 μ M BCAAs for 2 h in basal media, and Western blotting was performed on the indicated proteins. Vinculin was used as a loading control. One of four experiments is shown. **(F)** Ovar3 and Ovar10 cells were treated with the ATM inhibitor KU60019 (10 μ M) for 2 h in basal media, and Western blotting was performed on the indicated proteins. Vinculin was used as a loading control. One of three experiments is shown. **(G)** Fold change (Log_2FC) of metabolites in the ascites fluid in the indicated treatment groups.

Smida et al., 2016; Stagni et al., 2015; Tripathi et al., 2013; Viniegra et al., 2005). Similarly, how ATM inhibition promotes Rac1 activation, which is required for actin ruffling to initiate macropinosome formation, and whether this is dependent or independent of mTORC1 was not investigated in this study. Further research is warranted to better delineate this signaling pathway in ovarian cancer cells with inhibited ATM under nutrient-stress conditions.

Finally, we aimed to determine whether BCAA uptake is changed in ATM-inhibited tumors in vivo. To investigate

metabolite uptake from the microenvironment, we assessed metabolite abundance in the tumor, interstitial fluid, and ascites fluid, which commonly occurs in ovarian cancer models. Interstitial fluid and ascites fluid can be used to assess microenvironment metabolite abundance. While steady-state abundance of BCAAs in the tumor was not significantly changed (Table S1), BCAAs in the interstitial and ascites fluid were decreased upon treatment with the ATM inhibitor and increased in the combination group (Fig. 4 G, Fig. S4 G, and Table S1), suggesting that these metabolites are consumed by ATM inhibited tumors. Two

important caveats of these data are that the combination-treated tumors are dying, meaning that metabolite abundance may be due to a difference in survival and proliferation rather than a difference in metabolic preference. Additionally, we cannot rule out changes in microenvironmental BCAAs from other sources, such as metabolic changes in nontumor cells. Interestingly, other metabolites were altered in tumors treated with the ATM inhibitor (Fig. S4 H and Table S1), including nucleotides, which is consistent with our previous publication (Aird et al., 2015), and we and others have shown that mTORC1 activity directly promotes nucleotide synthesis (Ben-Sahra et al., 2013, 2016; Buj et al., 2019). Together, these data suggest other mechanisms are at play to promote metabolic adaptation under ATM-inhibited conditions. Future work will be aimed at further investigating these pathways.

In summary, we identified a new mechanism of macropinocytosis induction through the inhibition of ATM, which corresponds to a decrease in mTORC1 activity and an increase in the uptake of BCAAs. This study provides a novel mechanism of metabolism controlled by ATM inhibition and suggests that macropinocytosis represents a metabolic vulnerability that can be targeted in combination with ATM inhibitors, which have recently entered clinical trials (clinicaltrials.gov). Moreover, this pathway may also be a vulnerability of ATM-mutated- or low-expressing tumors. Since Ataxia telangiectasia (A-T) patients with ATM mutations also have metabolic disorders, our data may have implications beyond cancer for controlling metabolism in the context of low or mutated ATM.

Materials and methods

Cell lines and culture conditions

Ovcar8, Ovcar3, and Ovcar10 cells were cultured in RPMI-1640 (Cat# 10-040-CV; Corning) with 5% FBS. 293FT cells were cultured in DMEM (Cat# 10-013-CV; Corning) with 5% FBS. Normal diploid IMR90 (purchased from ATCC) was cultured in low oxygen (2% O₂) in DMEM (Cat# 10-017-CV; Corning) with 10% FBS supplemented with L-glutamine, nonessential amino acids, sodium pyruvate, and sodium bicarbonate. Experiments were performed on IMR90 between population doubling #25-35. All cell lines were cultured in MycoZap and were routinely tested for mycoplasma using a highly sensitive PCR-based method (Uphoff and Drexler, 2005). Tumor cell lines were authenticated using STR Profiling using Genetica DNA Laboratories.

Media conditions for experiments

The following media conditions were used for experiments, which are indicated in the figure legends: “replete media”: RPMI-1640 (Cat# 10-040-CV; Corning) supplemented with 5% FBS; “low serum media”: RPMI-1640 (Cat# 10-040-CV; Corning) supplemented with 0.1% FBS; “basal media”: Cat# D5030; Sigma-Aldrich without serum; “1% AA media” 1% AA media (99 parts D5030, 1 part complete RPMI-1640 + 5% FBS; final FBS = 0.05% FBS [Jayashankar and Edinger, 2020]).

Glucose uptake by flow cytometry

Cells (10⁵/well in 12-well plates) were incubated with 5 μM fluorescent glucose analog 2NBDG (N13195; Thermo Fisher

Scientific) in Opti-MEM I Reduced Serum Medium (31985088; Thermo Fisher Scientific) for 2 h. Cells were run on a 10-color FACSCanto flow cytometer (BD Biosciences). Data were analyzed with FlowJo Software.

YSI bioanalyzer analysis

Glucose and glutamine consumption was measured using a YSI 2950 Bioanalyzer (Yellow Springs). Briefly, the same number of cells (10⁵/well in 12-well plates) were seeded in complete media. One day later, the media was changed to RPMI-1640+0.1% FBS and the cells were incubated in 10 μM KU60019 (ApexBio) or 1 μM AZD0156 (ApexBio) for 24 h. Media was collected and the number of cells per well was counted to normalize for cell number.

Western blotting

Cell lysates were collected in 1× sample buffer (2% SDS, 10% glycerol, 0.01% bromophenol blue, 62.5 mM Tris, pH 6.8, 0.1M DTT) and boiled (10 min at 95°C). Protein concentration was determined using the Bradford assay. Proteins were resolved using SDS-PAGE gels and transferred to nitrocellulose membranes (Thermo Fisher Scientific; 110 mA for 2 h or overnight at 4°C). Membranes were blocked with 5% nonfat milk or 4% BSA in TBS containing 0.1% Tween-20 (TBS-T) for 1 h at room temperature. Membranes were incubated overnight at 4°C in primary antibodies (Table S2) in 4% BSA/TBS + 0.025% sodium azide. Membranes were washed four times in TBS-T for 5 min at room temperature after which they were incubated with HRP-conjugated secondary antibodies (Cell Signaling) for 1 h at room temperature. After washing four times in TBS-T for 5 min at room temperature, proteins were visualized on a film after incubation with SuperSignal West Pico PLUS Chemiluminescent Substrate (Thermo Fisher Scientific).

Lentiviral packaging and infection

Lentiviral constructs were transfected into 293FT cells using polyethylenimine (PEI). Lentivirus was packaged using the ViraPower Kit (Invitrogen) following the manufacturer’s instructions. Cells were infected overnight with lentivirus targeting the gene of interest or control shGFP and selected with 1 μg/ml puromycin for 3 d. The following shRNAs were used: shATM#1: TRCN0000038658; shATM#2: TRCN0000010299; shATR#1: TCRN0000039615; shATR#2: TCRN0000039616; shSLC2A1#1: TRCN0000043585; shSLC2A1#2: TRCN0000043584; shSLC2A4#1: TRCN0000043628; shSLC2A4#2: TRCN0000043629; shSLC1A5#1: TRCN0000043118; shSLC1A5#2: TRCN0000043119.

RT-qPCR

Total RNA was extracted from cells with Trizol, Dnase-treated, cleaned, and concentrated using Zymo columns (Cat# R1013; Zymo Research) following the manufacturer’s instructions. Optical density values of RNA were measured using NanoDrop One (Thermo Fisher Scientific) to confirm an A260 and A280 ratio above 1.9. Relative expression of target genes (Table S3) was analyzed using the QuantStudio 3 Real-Time PCR System (Thermo Fisher Scientific) with clear 96-well plates (Greiner Bio-One). Primers were designed using the Integrated DNA

Technologies (IDT) tool (<http://eu.idtdna.com/scitools/Applications/RealTimePCR/>). A total of 25 ng of RNA was used for One-Step qPCR (Quanta BioSciences) following the manufacturer's instructions in a final volume of 10 μ l. Conditions for amplification were 10 min at 48°C, 5 min at 95°C, 40 cycles of 10 s at 95°C, and 7 s at the corresponding annealing temperature (Table S3). The assay ended with a melting curve program: 15 s at 95°C, 1 min at 70°C, and then ramping to 95°C while continuously monitoring fluorescence. Each sample was assessed in triplicate. Relative quantification was determined to multiple reference genes (*B2M*, *MRPL9*, *PSMC4*, and *PUM1*) using the delta-delta Ct method.

Dextran uptake by flow cytometry

For Dextran-FITC experiments, cells were incubated with 1 or 5 mg/ml dextran-FITC (Cat # 90718-1G; Sigma-Aldrich) in the indicated media conditions. Where indicated, cells were incubated with 10 μ M KU60019, 25 μ M EIPA, 200 μ M BCAAs (mixture of valine [Cat # V0500-1G; Sigma-Aldrich], isoleucine [Cat # I2752-25G; Sigma-Aldrich], and leucine [Cat # L8000-1G; Sigma-Aldrich]), 2.5 μ M EHop-016 (Selleck Chemicals), 5 mM glucose, 1 mM pyruvate (Cat # 25-000-CI; Corning), 2 mM glutamine (Cat # G7513-100 ml; Sigma-Aldrich), 0.2 mM amino acids mixture (NEAAs, glutamine, BCAAs), or 0.1 mM NEAAs (Cat # 25-025-CI; Corning). For TMR-dextran, cells were incubated with 0.1 mg/ml TMR-dextran (Cat # D1818; Invitrogen) for 2 h. After washing once with 1 \times PBS, cells were incubated for 5 min in 0.1 M NaAc (pH 5.5) to quench dextran-FITC bound to the cell membrane. Cells were then trypsinized and run on a 10-color FACSCanto flow cytometer (BD Biosciences). For Annexin V/7AAD experiments, cells (2×10^4 /well in 12-well plates) were treated for 4 d with 2 μ M KU60019 and 2 μ M EIPA in RPMI + 5% FBS. Cells were stained with 2×10^6 cells/ml Annexin V (R37176; Thermo Fisher Scientific) and 0.5 μ g/ml 7AAD (13-6993-T200; Tonbo Biosciences) in 2.5 mM Ca²⁺-containing RPMI for 15 min at room temperature. Data were analyzed using FlowJo software. The percentage of high dextran uptake indicates the percentage of cells that demonstrate high dextran-FITC or dextran-TMR fluorescence. This was chosen as we observed a population of cells that had a larger uptake of dextran in microscopy experiments. The gating strategy for this can be found in Fig. S2 B.

Dextran uptake by fluorescence

Cells were incubated with 5 mg/ml dextran-FITC (Cat# 90718-1G; Sigma-Aldrich) in base media (D5030; Sigma-Aldrich) for 2 h. After washing once with 1 \times PBS, cells were incubated for 5 min in 0.1 M NaAc (pH 5.5) to quench dextran-FITC bound to the cell membrane. Cells were fixed in 4% paraformaldehyde (10 min) and permeabilized in 0.2% Triton X-100 (5 min). Cells were further incubated with 0.15 μ g/ml DAPI in PBS (1 min), mounted with fluorescence mounting medium (9 ml of glycerol [Fisher Scientific, BP229-1], 1 ml of 1 \times PBS, and 10 mg of p-phenylenediamine [EMD Chemicals Inc, PX0730]; pH was adjusted to a pH 8.0–9.0 using carbonate-bicarbonate buffer [0.2 M anhydrous sodium carbonate, 0.2 M sodium bicarbonate]), and sealed. For macropinoscytotic index, images were

acquired at room temperature using a Nikon Eclipse 90i microscope with a 20 \times /0.17 objective (Nikon DIC N2 Plan Apo) equipped with a CoolSNAP Photometrics camera and NIS-Elements software. The macropinoscytotic index was determined using the method described by Lee et al. (2019). Briefly, using ImageJ, background subtraction and threshold adjustments were performed. The number of macropinosomes was determined using the "Analyze Particles" feature in ImageJ, and the macropinoscytotic index was computed using the total particle area per cell. For the tumor model, 0.2 mg/mice Dextran, Oregon Green (D7173; Thermo Fisher Scientific) in 200 μ l Evans Blue dye (1% in sterile water; E2129; Sigma-Aldrich) was injected intraperitoneally 30 min prior to harvesting tumors. Tumors were frozen at -80°C in OCT (Tissue Tek) and sectioned using a cryostat. Tissues were incubated with 0.15 μ g/ml DAPI in PBS for 1 min, washed three times with PBS, mounted with the same media as above, and sealed. Images were acquired at room temperature using a confocal microscope (Leica SP8) with a 63 \times /1.4 HC PL APO oil objective and Leica Application Suite X (LAS X) software. The macropinoscytotic index was determined using the method described in Comisso et al. (2014), which was similar to above except that the macropinoscytotic index was computed using the area of each tumor field.

Crystal violet staining

Cells (10^5 /well in 12-well plates) were treated with the indicated concentrations KU60019, EIPA, or eHop-016 supplied daily in the indicated media. Cells were fixed in 1% paraformaldehyde (5 min) and stained with 0.05% crystal violet (20 min). Wells were destained for 5 min in 500 ml 10% acetic acid. Absorbance (590 nm) was measured using a spectrophotometer (Spectra Max 190). Each sample was assessed in triplicate.

Murine tumor model

2-mo-old female nude mice were purchased from Jackson Labs. All mice were maintained in a HEPA-filtered ventilated rack system at the Milton S. Hershey Medical Center animal facility. Mice were housed up to five mice per cage and in a 12-h light/dark cycle. This study was performed in strict accordance with the recommendations in the Guide for the Care and Use of Laboratory Animals of the National Institutes of Health. All experiments with animals were performed in accordance with institutional guidelines approved by the Institutional Animal Care and Use Committee (IACUC). Ovarian cancer cells (5×10^6 in 200 μ l PBS) were injected intraperitoneally into mice (eight mice per group based on pilot experiments). Mice were monitored every 3–4 d by noninvasive luciferase imaging by intraperitoneal injection of 150 mg/kg Luciferin (Perkin-Elmer) and quantification of luciferase activity using Imaging Systems (IVIS Spectrum System; Xenogen Corporation). On day 19, mice were randomized and thereafter treated daily with 10 mg/kg KU60019 and 10 mg/kg EIPA (both dissolved in DMSO/Tween 80/saline [10:10:80; v/v/v]) both alone and in combination via intraperitoneal injection daily. All animals were euthanized at day 48 after tumor implantation, and ascites fluid, interstitial fluid (Sullivan et al., 2019), and tumor tissues were collected.

IHC

IHC was conducted on formalin-fixed paraffin-embedded tissues using rabbit anti-cleaved caspase 3 antibody (1:300; Cat# 9661; Cell Signaling), EnVision+ Dual Link HRP secondary (Cat# K406311-2; Agilent), and the ImmPACT DAB Peroxidase (HRP) Substrate (Cat# SK-4105; Vector Laboratories) following the manufacturer's instructions. Briefly, the tissue was rehydrated by incubating in a series of zylens/ethanol baths. Antigen retrieval was performed by steaming in citrate buffer (Cat# 005000; Thermo Fisher Scientific) for 40 min. Endogenous peroxidase was quenched by incubating in 3% H₂O₂/MeOH for 20 min after which slides were washed and blocked in 1% BSA/PBS at room temperature for 30 min. Slides were incubated overnight at 4°C in primary antibody (1:300), washed, and incubated in secondary-HRP for 45 min. DAB was used to develop, and Mayer's Hemotoxylin (Cat# MHS16; Sigma-Aldrich) was used to counterstain the tissue. Finally, slides were dehydrated and mounted using Cytoseal. Images were acquired at room temperature using a Nikon Ti2-E microscope with a 10×/0.45 objective (Nikon CFI Plan APO Lambda) equipped with a DS-FI3 camera and NIS-Elements software. H score was determined on blinded samples, where H score = [1 × (% cells 1+) + 2 × (% cells 2+) + 3 × (% cells 3+)].

Metabolomics

Metabolomic profiling was conducted using ion-pairing reversed-phase liquid chromatography-high resolution mass spectrometry (LC-HRMS) modified from previous methods for polar analytes (Guo et al., 2016) and nucleotides (Kuskovsky et al., 2019). Samples were spiked with a stable isotope mix containing AMP-¹³C₁₀,¹⁵N₅, dAMP-¹³C₁₀,¹⁵N₅, ATP-¹³C₁₀,¹⁵N₅, dATP-¹³C₁₀,¹⁵N₅, dTMP-¹³C₁₀,¹⁵N₂, dTTP-¹³C₁₀,¹⁵N₂, dCMP-¹³C₉,¹⁵N₃, CTP-¹³C₉,¹⁵N₃, dCTP-¹³C₉,¹⁵N₃, ¹³C₃-sodium pyruvate, ¹³C₃-lactate, ¹³C₄-fumaric acid, ¹³C₄-succinic acid, ¹³C₄¹⁵N₁-aspartic acid, ¹³C₆-citric acid, ¹³C₆-glucose-6-phosphate, ¹³C₂-acetylCoA, ¹³C₅-D-α-hydroxyglutaric acid, ¹³C₅¹⁵N₂-glutamine from Sigma-Aldrich or Cambridge Isotope Laboratories. 1 ml of Optima LC-MS grade 80:20 methanol/water prechilled to -80°C was then added to each sample, followed by 30-s vortex mixing, 15-s pulse sonication with a probe tip sonicator, and then the samples were returned to the -80°C freezer for 30 min. Insoluble debris was precipitated by centrifugation for 10 min, 17,000×g at 4°C. The supernatant was evaporated to dryness under nitrogen, resuspended in 100 μl 5% 5-sulfosalicylic acid in water, and 5 μl was injected for analysis. LC-HRMS was conducted on an Ultimate 3000 UHPLC equipped with a refrigerated autosampler (at 6°C) and a column heater (at 55°C) with a HSS C18 column (2.1 × 100 mm i.d., 3.5 μm; Waters) used for separations. Solvent A was 5 mM DIPEA and 200 mM HFIP, and solvent B was methanol with 5 mM DIPEA 200 mM HFIP. The gradient was as follows: 100% A for 3 min at 0.18 ml/min, 100% A at 6 min with 0.2 ml/min, 98% A at 8 min with 0.2 ml/min, 86% A at 12 min with 0.2 ml/min, 40% A at 16 min, and 1% A at 17.9–18.5 min with 0.3 ml/min then increased to 0.4 ml/min until 20 min. The flow was ramped down to 0.18 ml/min back to 100% A over a 5 min re-equilibration. For MS analysis, the UHPLC was coupled to a Q Exactive HF mass spectrometer (Thermo Fisher Scientific) equipped with a HESI II source

operating in negative mode. The operating conditions were as follows: spray voltage 4000 V; vaporizer temperature 200°C; capillary temperature 350°C; S-lens 60; in-source CID 1.0 eV, and resolution 60,000. The sheath gas (nitrogen) and auxiliary gas (nitrogen) pressures were 45 and 10 (arbitrary units), respectively. Single ion monitoring (SIM) windows were acquired around the [M-H]⁻ of each analyte with a 20 m/z isolation window, 4 m/z isolation window offset, 1e⁶ ACG target and 80 ms IT, alternating in a Full MS scan from 70 to 950 m/z with 1e6 ACG and 100 ms IT. Data were analyzed in XCalibur v4.0 and/or Tracefinder v4.1 (Thermo Fisher Scientific) using a 5 ppm window for integration of the peak area of all analytes and internal standards used for normalization. For BCAA labeling experiments, cells were incubated for 2 h with 100 μM labeled BCAAs [Cambridge Isotope Laboratories: L-LEUCINE (13C6, 99%; 15N, 99%), Cat# CNLM-281-H; L-ISOLEUCINE (13C6, 99%; 15N, 99%), Cat# CNLM-561-H; L-VALINE (13C5, 99%; 15N, 99%), Cat# CNLM-442-H)]. Mass spectrometry methods are described above. Pool size in labeling experiments was calculated as the sum of peak areas of all isotopologs (including 13C and 15N). Isotopolog enrichment was calculated by FluxFix (Trefely et al., 2016). For targeted BCAA quantification in unlabeled conditions, the method was the same, except that samples were spiked with ¹³C₆¹⁵N-leucine and ¹³C₅¹⁵N-valine before extraction, and analysis was conducted using the ratio of the BCAAs to their labeled internal standards.

Quantification and statistical analysis

GraphPad Prism version 9.0 was used to perform statistical analysis. One-way ANOVA or unpaired, two-sided *t* tests were used as appropriate to determine the P values of raw data. Data distribution was assumed to be normal, but this was not formally tested. Longitudinal and cross-sectional analysis of tumor volume were calculated using TumorGrowth tool using default parameters (Enot et al., 2018). P values <0.05 were considered significant.

Online supplemental material

Fig. S1 (complementary to Fig. 1) shows that inhibition of ATM in additional cell lines increases glucose and glutamine consumption, and parental cell lines expressing shRNA against GLUT1, GLUT4, or SLC2A4 have decreased uptake of glucose or glutamine. Fig. S2 (complementary to Fig. 2) shows that inhibition or knockdown of ATM, but not ATR, increases macropinocytosis. Fig. S3 (complementary to Fig. 3) shows that the combination of ATM inhibitor and macropinocytosis inhibitor is synergistic in additional cell lines and different media conditions. Fig. S4 (complementary to Fig. 4) shows that the relative abundance of BCAAs is increased by ATM inhibition and decreased by EIPA in vitro. Fig. S4 also shows the tumor metabolites in different conditions. Table S1 shows the tumor, ascites, and interstitial fluid metabolite data associated with Fig. 4 G; and Fig. S4, G and H. Table S2 is the list of the antibodies used in this study. Table S3 is a list of primers used for this study.

Acknowledgments

This work was supported by grants from the National Institutes of Health (F31CA236372 to E.S. Dahl, F31CA250366 to K.E. Leon,

R01GM132261 to N.W. Snyder, R37CA240625 and R00CA194309 to K.M. Aird, and R01CA259111 to N.W. Snyder and K.M. Aird), the Congressionally Directed Medical Research Program (W81XWH-18-1-0103 and W81XWH-21-1-0840 to K.M. Aird), a Penn State Cancer Institute Postdoctoral Fellowship (R. Buj), and a HERA Ovarian Cancer Foundation Grant (N.K. Tangudu). This project used the Hillman Cytometry Facility, which is supported in part by award P30CA047904 from the National Institutes of Health.

The authors declare no competing financial interests.

Author contributions: Conceptualization, K.M. Aird; Methodology, E.L. Varner, E. von Krusenstiern, and N.W. Snyder; Investigation, Z. Huang, C.W. Chen, R. Buj, N.K. Tangudu, R. Fang, K.E. Leon, E.S. Dahl, E.L. Varner, E. von Krusenstiern, N.W. Snyder, and K.M. Aird; Writing, K.M. Aird; Visualization, K.M. Aird; Supervision, N.W. Snyder and K.M. Aird; Funding acquisition, N.W. Snyder and K.M. Aird.

Submitted: 6 July 2020

Revised: 30 May 2022

Accepted: 6 October 2022

References

Aird, K.M., A.J. Worth, N.W. Snyder, J.V. Lee, S. Sivanand, Q. Liu, I.A. Blair, K.E. Wellen, and R. Zhang. 2015. ATM couples replication stress and metabolic reprogramming during cellular senescence. *Cell Rep.* 11: 893–901. <https://doi.org/10.1016/j.celrep.2015.04.014>

Alexander, A., S.L. Cai, J. Kim, A. Namez, M. Sahin, K.H. MacLean, K. Inoki, K.L. Guan, J. Shen, M.D. Person, et al. 2010. ATM signals to TSC2 in the cytoplasm to regulate mTORC1 in response to ROS. *Proc. Natl. Acad. Sci. USA.* 107:4153–4158. <https://doi.org/10.1073/pnas.0913860107>

Batey, M.A., Y. Zhao, S. Kyle, C. Richardson, A. Slade, N.M.B. Martin, A. Lau, D.R. Newell, and N.J. Curtin. 2013. Preclinical evaluation of a novel ATM inhibitor, KU59403, in vitro and in vivo in p53 functional and dysfunctional models of human cancer. *Mol. Cancer Ther.* 12:959–967. <https://doi.org/10.1158/1535-7163.MCT-12-0707>

Ben-Sahra, I., J.J. Howell, J.M. Asara, and B.D. Manning. 2013. Stimulation of de novo pyrimidine synthesis by growth signaling through mTOR and S6K1. *Science.* 339:1323–1328. <https://doi.org/10.1126/science.1228792>

Ben-Sahra, I., G. Hoxhaj, S.J.H. Ricault, J.M. Asara, and B.D. Manning. 2016. mTORC1 induces purine synthesis through control of the mitochondrial tetrahydrofolate cycle. *Science.* 351:728–733. <https://doi.org/10.1126/science.1260489>

Buj, R., C.W. Chen, E.S. Dahl, K.E. Leon, R. Kuskovsky, N. Maglakelidze, M. Navaratnarajah, G. Zhang, M.T. Doan, H. Jiang, et al. 2019. Suppression of p16 induces mTORC1-mediated nucleotide metabolic reprogramming. *Cell Rep.* 28:1971–1980.e8. <https://doi.org/10.1016/j.celrep.2019.07.084>

Cantor, J.R. 2019. The rise of physiologic media. *Trends Cell Biol.* 29:854–861. <https://doi.org/10.1016/j.tcb.2019.08.009>

Chen, A.K., Z. Cheng, M.A. Behlke, and A. Tsourkas. 2008. Assessing the sensitivity of commercially available fluorophores to the intracellular environment. *Anal. Chem.* 80:7437–7444. <https://doi.org/10.1021/ac8011347>

Chen, C.W., R. Buj, E.S. Dahl, K.E. Leon, and K.M. Aird. 2020. ATM inhibition synergizes with fenofibrate in high grade serous ovarian cancer cells. *Heliyon.* 6:e05097. <https://doi.org/10.1016/j.heliyon.2020.e05097>

Commisso, C., S.M. Davidson, R.G. Soydaner-Azeloglu, S.J. Parker, J.J. Kamphorst, S. Hackett, E. Grabocka, M. Nofal, J.A. Drebin, C.B. Thompson, et al. 2013. Macropinocytosis of protein is an amino acid supply route in Ras-transformed cells. *Nature.* 497:633–637. <https://doi.org/10.1038/nature12138>

Commisso, C., R.J. Flinn, and D. Bar-Sagi. 2014. Determining the macropinocytic index of cells through a quantitative image-based assay. *Nat. Protoc.* 9:182–192. <https://doi.org/10.1038/nprot.2014.004>

Cosentino, C., D. Grieco, and V. Costanzo. 2011. ATM activates the pentose phosphate pathway promoting anti-oxidant defence and DNA repair. *EMBO J.* 30:546–555. <https://doi.org/10.1038/emboj.2010.330>

Dahl, E.S., and K.M. Aird. 2017. Ataxia-telangiectasia mutated modulation of carbon metabolism in cancer. *Front. Oncol.* 7:291. <https://doi.org/10.3389/fonc.2017.00291>

Dai, M., G. Yan, N. Wang, G. Daliah, A.M. Edick, S. Poulet, J. Boudreault, S. Ali, S.A. Burgos, and J.J. Lebrun. 2021. In vivo genome-wide CRISPR screen reveals breast cancer vulnerabilities and synergistic mTOR/Hippo targeted combination therapy. *Nat. Commun.* 12:3055. <https://doi.org/10.1038/s41467-021-23316-4>

Davidson, S.M., O. Jonas, M.A. Keibler, H.W. Hou, A. Luengo, J.R. Mayers, J. Wyckoff, A.M. Del Rosario, M. Whitman, C.R. Chin, et al. 2017. Direct evidence for cancer-cell-autonomous extracellular protein catabolism in pancreatic tumors. *Nat. Med.* 23:235–241. <https://doi.org/10.1038/nm.4256>

Dendo, K., T. Yugawa, T. Nakahara, S.I. Ohno, N. Goshima, H. Arakawa, and T. Kiyono. 2018. Induction of non-apoptotic programmed cell death by oncogenic RAS in human epithelial cells and its suppression by MYC overexpression. *Carcinogenesis.* 39:202–213. <https://doi.org/10.1093/carcin/bgx124>

Enot, D.P., E. Vacchelli, N. Jacquilot, L. Zitvogel, and G. Kroemer. 2018. TumGrowth: An open-access web tool for the statistical analysis of tumor growth curves. *Oncotarget.* 7:e1462431. <https://doi.org/10.1080/2162402X.2018.1462431>

Foster, K.G., and D.C. Fingar. 2010. Mammalian target of rapamycin (mTOR): Conducting the cellular signaling symphony. *J. Biol. Chem.* 285: 14071–14077. <https://doi.org/10.1074/jbc.R109.094003>

Fujii, M., K. Kawai, Y. Egami, and N. Araki. 2013. Dissecting the roles of Rac1 activation and deactivation in macropinocytosis using microscopic photo-manipulation. *Sci. Rep.* 3:2385. <https://doi.org/10.1038/srep02385>

Fujimaki, S., Y. Matsuda, T. Wakai, A. Sanpei, M. Kubota, M. Takamura, S. Yamagiwa, M. Yano, S. Ohkoshi, and Y. Aoyagi. 2012. Blockade of ataxia telangiectasia mutated sensitizes hepatoma cell lines to sorafenib by interfering with Akt signaling. *Cancer Lett.* 319:98–108. <https://doi.org/10.1016/j.canlet.2011.12.043>

Golding, S.E., E. Rosenberg, B.R. Adams, S. Wignarajah, J.M. Beckta, M.J. O'Connor, and K. Valerie. 2012. Dynamic inhibition of ATM kinase provides a strategy for glioblastoma multiforme radiosensitization and growth control. *Cell Cycle.* 11:1167–1173. <https://doi.org/10.4161/cc.11.6.19576>

Guleria, A., and S. Chandna. 2016. ATM kinase: Much more than a DNA damage responsive protein. *DNA Repair.* 39:1–20. <https://doi.org/10.1016/j.dnarep.2015.12.009>

Guo, L., A.J. Worth, C. Mesaros, N.W. Snyder, J.D. Glickson, and I.A. Blair. 2016. Diisopropylethylamine/hexafluoroisopropanol-mediated ion-pairing ultra-high-performance liquid chromatography/mass spectrometry for phosphate and carboxylate metabolite analysis: Utility for studying cellular metabolism. *Rapid Commun. Mass Spectrom.* 30: 1835–1845. <https://doi.org/10.1002/rcm.7667>

Hobbs, G.A., and C.J. Der. 2022. KRAS^{G12R}-Independent macropinocytosis in pancreatic cancer. *Sub Cell. Biochem.* 98:205–221. https://doi.org/10.1007/978-3-030-94004-1_11

Hodakoski, C., B.D. Hopkins, G. Zhang, T. Su, Z. Cheng, R. Morris, K.Y. Rhee, M.D. Goncalves, and L.C. Cantley. 2019. Rac-mediated macropinocytosis of extracellular protein promotes glucose independence in non-small cell lung cancer. *Cancers.* 11:37. <https://doi.org/10.3390/cancers11010037>

Ivanov, A.I. 2008. Pharmacological inhibition of endocytic pathways: Is it specific enough to be useful?. *Methods Mol. Biol.* 440:15–33. https://doi.org/10.1007/978-1-59745-178-9_2

Jayashankar, V., and A.L. Edinger. 2020. Macropinocytosis confers resistance to therapies targeting cancer anabolism. *Nature Commun.* 11:1121. <https://doi.org/10.1038/s41467-020-14928-3>

Jin, M.H., and D.Y. Oh. 2019. ATM in DNA repair in cancer. *Pharmacol. Ther.* 203:107391. <https://doi.org/10.1016/j.pharmthera.2019.07.002>

Kamphorst, J.J., M. Nofal, C. Commisso, S.R. Hackett, W. Lu, E. Grabocka, M.G. Vander Heiden, G. Miller, J.A. Drebin, D. Bar-Sagi, et al. 2015. Human pancreatic cancer tumors are nutrient poor and tumor cells actively scavenge extracellular protein. *Cancer Res.* 75:544–553. <https://doi.org/10.1158/0008-5472.CAN-14-2211>

Kim, J., and K.L. Guan. 2019. mTOR as a central hub of nutrient signalling and cell growth. *Nat. Cell Biol.* 21:63–71. <https://doi.org/10.1038/s41556-018-0205-1>

Kim, S.M., T.T. Nguyen, A. Ravi, P. Kubiniok, B.T. Finicle, V. Jayashankar, L. Malacrida, J. Hou, J. Robertson, D. Gao, et al. 2018. PTEN deficiency and AMPK activation promote nutrient scavenging and anabolism in prostate cancer cells. *Cancer Discov.* 8:866–883. <https://doi.org/10.1158/2159-8290.CD-17-1215>

- King, J.S., and R.R. Kay. 2019. The origins and evolution of macropinocytosis. *Philos. Trans. R. Soc. Lond. Ser. B. Biol. Sci.* 374:20180158. <https://doi.org/10.1098/rstb.2018.0158>
- Kuskovskiy, R., R. Buj, P. Xu, S. Hofbauer, M.T. Doan, H. Jiang, A. Bostwick, C. Mesaros, K.M. Aird, and N.W. Snyder. 2019. Simultaneous isotope dilution quantification and metabolic tracing of deoxyribonucleotides by liquid chromatography high resolution mass spectrometry. *Anal. Biochem.* 568:65–72. <https://doi.org/10.1016/j.ab.2018.12.023>
- Lambies, G., and C. Commisso. 2022. Macropinocytosis and cancer: From tumor stress to signaling pathways. *Sub Cell. Biochem.* 98:15–40. https://doi.org/10.1007/978-3-030-94004-1_2
- Lee, S.W., Y. Zhang, M. Jung, N. Cruz, B. Alas, and C. Commisso. 2019. EGFR-pak signaling selectively regulates glutamine deprivation-induced macropinocytosis. *Dev. Cell.* 50:381–392.e5. <https://doi.org/10.1016/j.devcel.2019.05.043>
- McKinnon, P.J. 2004. ATM and ataxia telangiectasia. *EMBO Rep.* 5:772–776. <https://doi.org/10.1038/sj.embor.7400210>
- McKinnon, P.J. 2012. ATM and the molecular pathogenesis of ataxia telangiectasia. *Annu. Rev. Pathol.* 7:303–321. <https://doi.org/10.1146/annurev-pathol-011811-132509>
- Meng, D., Q. Yang, M.H. Jeong, A. Curukovic, S. Tiwary, C.H. Melick, T.D. Lama-Sherpa, H. Wang, M. Huerta-Rosario, G. Urquhart, et al. 2022. SNAT7 regulates mTORC1 via macropinocytosis. *Proc. Natl. Acad. Sci. USA.* 119:e2123261119. <https://doi.org/10.1073/pnas.2123261119>
- Nofal, M., K. Zhang, S. Han, and J.D. Rabinowitz. 2017. mTOR inhibition restores amino acid balance in cells dependent on catabolism of extracellular protein. *Mol. Cell.* 67:936–946.e5. <https://doi.org/10.1016/j.molcel.2017.08.011>
- Pacitto, R., I. Gaeta, J.A. Swanson, and S. Yoshida. 2017. CXCL12-induced macropinocytosis modulates two distinct pathways to activate mTORC1 in macrophages. *J. Leukoc. Biol.* 101:683–692. <https://doi.org/10.1189/jlb.2A0316-141RR>
- Palm, W. 2019. Metabolic functions of macropinocytosis. *Philos. Trans. R. Soc. Lond. Ser. B. Biol. Sci.* 374:20180285. <https://doi.org/10.1098/rstb.2018.0285>
- Palm, W. 2022. Signaling pathways that regulate macropinocytosis in mammalian cells. *Sub Cell. Biochem.* 98:143–167. https://doi.org/10.1007/978-3-030-94004-1_8
- Palm, W., J. Araki, B. King, R.G. DeMatteo, and C.B. Thompson. 2017. Critical role for PI3-kinase in regulating the use of proteins as an amino acid source. *Proc. Natl. Acad. Sci. USA.* 114:E8628–E8636. <https://doi.org/10.1073/pnas.1712726114>
- Palm, W., Y. Park, K. Wright, N.N. Pavlova, D.A. Tuveson, and C.B. Thompson. 2015. The utilization of extracellular proteins as nutrients is suppressed by mTORC1. *Cell.* 162:259–270. <https://doi.org/10.1016/j.cell.2015.06.017>
- Perera, R.M., and R. Zoncu. 2016. The lysosome as a regulatory hub. *Annu. Rev. Cell Dev. Biol.* 32:223–253. <https://doi.org/10.1146/annurev-cellbio-111315-125125>
- Recouvreux, M.V., and C. Commisso. 2017. Macropinocytosis: A metabolic adaptation to nutrient stress in cancer. *Front. Endocrinol.* 8:261. <https://doi.org/10.3389/fendo.2017.00261>
- Redelman-Sidi, G., A. Binyamin, I. Gaeta, W. Palm, C.B. Thompson, P.B. Rommesser, S.W. Lowe, M. Bagul, J.G. Doench, D.E. Root, and M.S. Glickman. 2018. The canonical Wnt pathway drives macropinocytosis in cancer. *Cancer Res.* 78:4658–4670. <https://doi.org/10.1158/0008-5472.CAN-17-3199>
- Riches, L.C., A.G. Trinidad, G. Hughes, G.N. Jones, A.M. Hughes, A.G. Thomason, P. Gavine, A. Cui, S. Ling, J. Stott, et al. 2020. Pharmacology of the ATM inhibitor AZD0156: Potentiation of irradiation and olaparib responses preclinically. *Mol. Cancer Ther.* 19:13–25. <https://doi.org/10.1158/1535-7163.MCT-18-1394>
- Saxton, R.A., and D.M. Sabatini. 2017. mTOR signaling in growth, metabolism, and disease. *Cell.* 169:361–371. <https://doi.org/10.1016/j.cell.2017.03.035>
- Shiloh, Y. 2003. ATM and related protein kinases: Safeguarding genome integrity. *Nat. Rev. Cancer* 3:155–168. <https://doi.org/10.1038/nrc1011>
- Sivanand, S., and M.G. Vander Heiden. 2020. Emerging roles for branched-chain amino acid metabolism in cancer. *Cancer Cell.* 37:147–156. <https://doi.org/10.1016/j.ccell.2019.12.011>
- Smida, M., F. Fece de la Cruz, C. Kerzendorfer, I.Z. Uras, B. Mair, A. Mazouzi, T. Suchankova, T. Konopka, A.M. Katz, K. Paz, et al. 2016. MEK inhibitors block growth of lung tumours with mutations in ataxia-telangiectasia mutated. *Nat. Commun.* 7:13701. <https://doi.org/10.1038/ncomms13701>
- Stagni, V., I. Manni, V. Oropallo, M. Mottolese, A. Di Benedetto, G. Piaggio, R. Falcioni, D. Giaccari, S. Di Carlo, F. Sperati, et al. 2015. ATM kinase sustains HER2 tumorigenicity in breast cancer. *Nat. Commun.* 6:6886. <https://doi.org/10.1038/ncomms7886>
- Su, H., F. Yang, R. Fu, X. Li, R. French, E. Mose, X. Pu, B. Trinh, A. Kumar, J. Liu, et al. 2021. Cancer cells escape autophagy inhibition via NRF2-induced macropinocytosis. *Cancer Cell.* 39:678–693.e11. <https://doi.org/10.1016/j.ccell.2021.02.016>
- Sullivan, M.R., L.V. Danai, C.A. Lewis, S.H. Chan, D.Y. Gui, T. Kunchok, E.A. Dennstedt, M.G. Vander Heiden, and A. Muir. 2019. Quantification of microenvironmental metabolites in murine cancers reveals determinants of tumor nutrient availability. *Elife.* 8:e44235. <https://doi.org/10.7554/eLife.44235>
- Sung, S., J. Choi, and H. Cheong. 2015. Catabolic pathways regulated by mTORC1 are pivotal for survival and growth of cancer cells expressing mutant Ras. *Oncotarget.* 6:40405–40417. <https://doi.org/10.18632/oncotarget.6334>
- Tejeda-Munoz, N., L.V. Albrecht, M.H. Bui, and E.M. De Robertis. 2019. Wnt canonical pathway activates macropinocytosis and lysosomal degradation of extracellular proteins. *Proc. Natl. Acad. Sci. USA.* 6:40405–40417. <https://doi.org/10.18632/oncotarget.6334>
- Trefely, S., P. Ashwell, and N.W. Snyder. 2016. FluxFix: Automatic isotopologue normalization for metabolic tracer analysis. *BMC Bioinf.* 17:485. <https://doi.org/10.1186/s12859-016-1360-7>
- Tripathi, D.N., R. Chowdhury, L.J. Trudel, A.R. Tee, R.S. Slack, C.L. Walker, and G.N. Wogan. 2013. Reactive nitrogen species regulate autophagy through ATM-AMPK-TSC2-mediated suppression of mTORC1. *Proc. Natl. Acad. Sci. USA.* 110:E2950–E2957. <https://doi.org/10.1073/pnas.1307736110>
- Uphoff, C.C., and H.G. Drexler. 2013. Detection of mycoplasma contaminations. *Methods Mol. Biol.* 946:1–13. https://doi.org/10.1007/978-1-62703-128-8_1
- Valentin-Vega, Y.A., K.H. Maclean, J. Tait-Mulder, S. Milasta, M. Steeves, F.C. Dorsey, J.L. Cleveland, D.R. Green, and M.B. Kastan. 2012. Mitochondrial dysfunction in ataxia-telangiectasia. *Blood.* 119:1490–1500. <https://doi.org/10.1182/blood-2011-08-373639>
- Viniegua, J.G., N. Martínez, P. Modirassari, J. Hernández Losa, C. Parada Cobo, V.J. Sánchez-Arévalo Lobo, C.I. Aceves Luquero, L. Alvarez-Valina, S. Ramón y Cajal, J.M. Rojas, and R. Sánchez-Prieto. 2005. Full activation of PKB/Akt in response to insulin or ionizing radiation is mediated through ATM. *J. Biol. Chem.* 280:4029–4036. <https://doi.org/10.1074/jbc.M410344200>
- Weber, A.M., and A.J. Ryan. 2015. ATM and ATR as therapeutic targets in cancer. *Pharmacol. Ther.* 149:124–138. <https://doi.org/10.1016/j.pharmthera.2014.12.001>
- Yao, W., J.L. Rose, W. Wang, S. Seth, H. Jiang, A. Taguchi, J. Liu, L. Yan, A. Kapoor, P. Hou, et al. 2019. Syndecan 1 is a critical mediator of macropinocytosis in pancreatic cancer. *Nature.* 568:410–414. <https://doi.org/10.1038/s41586-019-1062-1>
- Yoshida, S., R. Pacitto, Y. Yao, K. Inoki, and J.A. Swanson. 2015. Growth factor signaling to mTORC1 by amino acid-laden macropinosomes. *J. Cell Biol.* 211:159–172. <https://doi.org/10.1083/jcb.201504097>
- Zhang, M.S., J.D. Cui, D. Lee, V.W.H. Yuen, D.K.C. Chiu, C.C. Goh, J.W.S. Cheu, A.P.W. Tse, M.H.R. Bao, B.P.Y. Wong, et al. 2022. Hypoxia-induced macropinocytosis represents a metabolic route for liver cancer. *Nature Commun.* 13:954. <https://doi.org/10.1038/s41467-022-28618-9>
- Zhang, Y., and C. Commisso. 2019. Macropinocytosis in cancer: A complex signaling network. *Trends Cancer.* 5:332–334. <https://doi.org/10.1016/j.trecan.2019.04.002>

Supplemental material

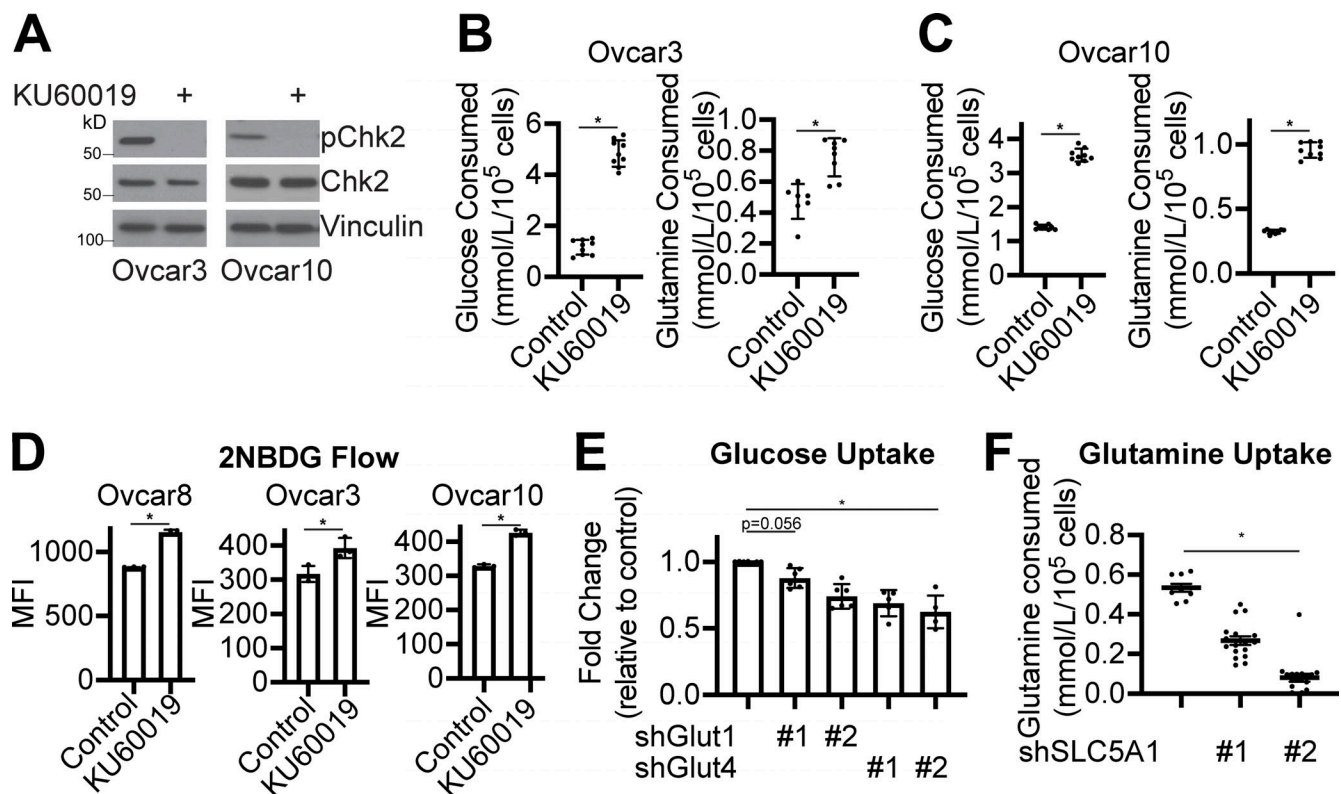


Figure S1. Inhibition of ATM increases glucose and glutamine consumption in multiple cell lines; related to Fig. 1. (A) Ovar3 and Ovar10 cells were treated with the ATM inhibitor KU60019 (10 μ M) for 24 h in RPMI-1640 + 1% FBS. pChk2 and total Chk2 expression were determined by immunoblotting. Vinculin was used as a loading control. One of three experiments is shown. (B) Ovar3 cells were treated with the ATM inhibitor KU60019 (10 μ M) for 24 h in RPMI-1640 + 1% FBS, and glucose and glutamine consumption was determined. $n = 9$ /group, one of two experiments is shown. Data represent mean \pm SD. * $P < 0.005$; unpaired two-sided t test. (C) Same as B, but for Ovar10 cells. (D) Glucose uptake in the indicated cells by 2NBDG was determined by flow cytometry after treatment with the ATM inhibitor KU60019 (10 μ M) for 24 h in RPMI-1640 + 1% FBS. MFI = median fluorescence intensity. $n = 3$ /group, one of at least two experiments is shown. Data represent mean \pm SD. * $P < 0.05$; unpaired two-sided t test. (E) Parental Ovar3 cells were infected with lentivirus expressing short hairpin RNAs (shRNAs) targeting *SLC2A1* (GLUT1) or *SLC2A4* (GLUT4). shGFP was used as a control. Glucose uptake was determined using the fluorescent glucose analog 2NBDG by flow cytometry. $n = 6$ /group, one of two experiments is shown. Data represent mean \pm SD. * $P < 0.0001$ vs. control; one-way ANOVA. (F) Parental Ovar8 cells were infected with lentivirus expressing shRNAs targeting *SLC1A5*. shGFP was used as a control. Glutamine uptake was determined. $n = 9$ /group, one of two experiments is shown. Data represent mean \pm SEM. * $P < 0.0001$ vs. control; one-way ANOVA.

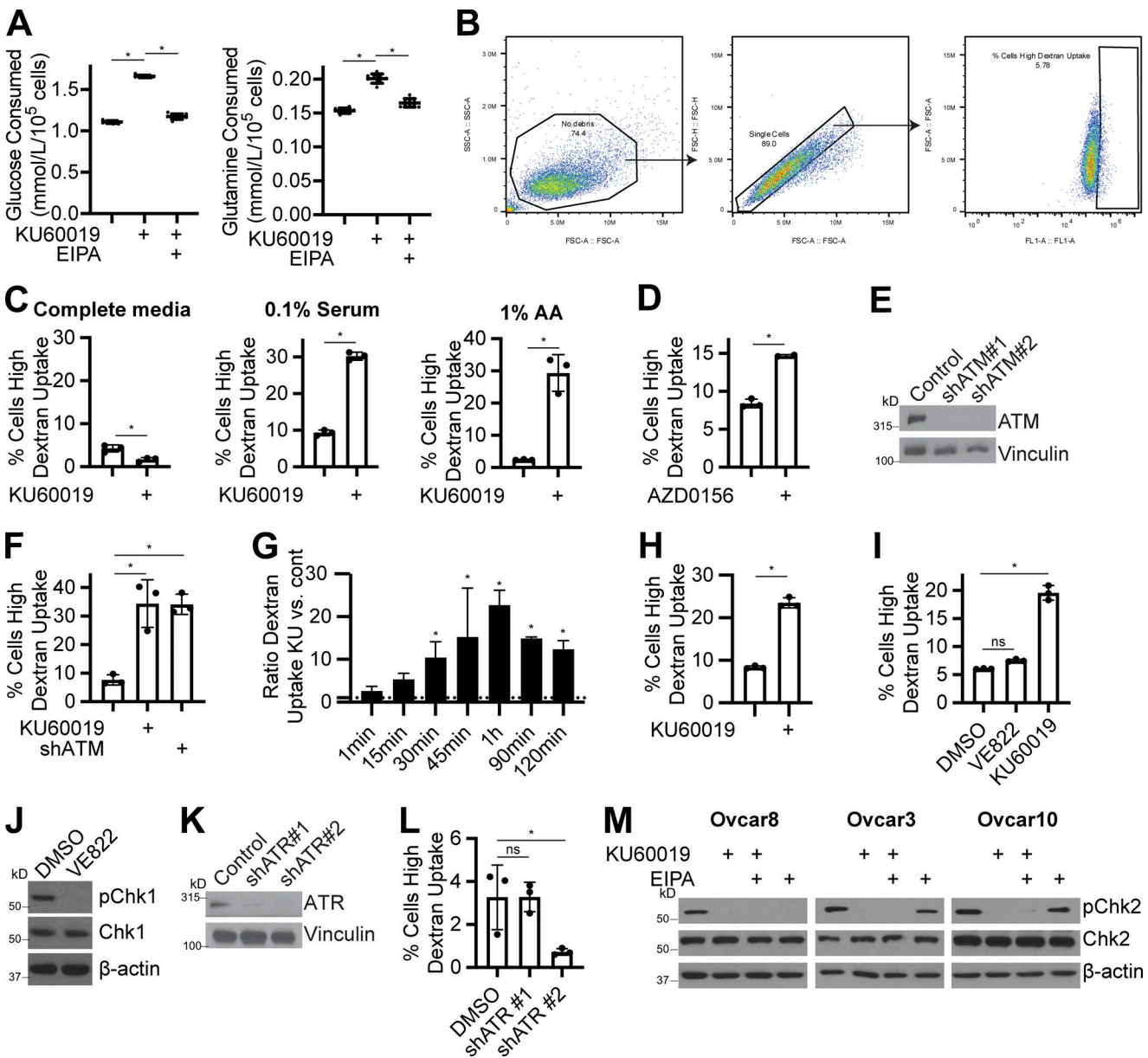


Figure S2. **Inhibition of ATM, but not ATR, induces macropinocytosis; related to Fig. 2.** (A) Ovarc8 cells were treated with the ATM inhibitor KU60019 (10 μ M) in combination with EIPA (25 μ M) for 24 h in RPMI-1640 + 0.1% FBS. Glucose and glutamine uptake were determined. $n = 9$ /group, one of three experiments is shown. Data represent mean \pm SD. * $P < 0.005$; unpaired two-sided t test. (B) Gating strategy for dextran uptake flow cytometry experiments is shown. (C) Ovarc8 cells were treated with the ATM inhibitor KU60019 (10 μ M) for 2 h using the indicated media conditions and dextran uptake was determined by flow cytometry. $N = 3$ /group, one of three experiments is shown. Data represent mean \pm SD. * $P < 0.01$; unpaired two-sided t test. (D) Ovarc8 cells were treated with the ATM inhibitor AZD0156 (1 μ M) for 2 h in basal media, and dextran uptake was determined by flow cytometry. $n = 3$ /group, one of three experiments is shown. Data represent mean \pm SD. * $P < 0.005$; unpaired two-sided t test. (E and F) Ovarc8 cells were infected with lentivirus expressing short hairpin RNAs (shRNAs) targeting ATM. shGFP was used as a control. (E) Immunoblot analysis of ATM. Vinculin was used as a loading control. One of five experiments is shown. (F) Dextran uptake in basal media was determined by flow cytometry. $n = 3$ /group, one of five experiments is shown. Data represent mean \pm SD. * $P < 0.0001$ vs. control; one-way ANOVA. (G) Ovarc8 cells were treated with the ATM inhibitor KU60019 (10 μ M) for the indicated time points in basal media, and dextran uptake was determined by flow cytometry. Data shown are the ratio of % cells with high dextran uptake in KU60019-treated cells vs. vehicle controls at each time point. $n = 3$ /group. Data represent mean \pm SD. * $P < 0.0001$ vs. controls; unpaired two-sided t test. (H) Ovarc8 cells were treated with the ATM inhibitor KU60019 (10 μ M) for 2 h in basal media, and 70 kD TMR-dextran uptake was determined by flow cytometry. $N = 3$ /group, one of three experiments is shown. Data represent mean \pm SD. * $P < 0.0001$; unpaired two-sided t test. (I–J) Ovarc8 cells were treated with the ATR inhibitor VE822 (1 μ M) for 2 h in basal media. (I) Dextran uptake was determined by flow cytometry. $n = 3$ /group, one of three experiments is shown. Data represent mean \pm SD. ns = not significant; unpaired two-sided t test. (J) Immunoblot analysis of p-Chk1 and total Chk1. β -actin was used as a loading control. One of three experiments is shown. (K and L) Ovarc8 cells were infected with lentivirus expressing short hairpin RNAs (shRNAs) targeting ATR. shGFP was used as a control. (K) Immunoblot analysis of ATR. Vinculin was used as a loading control. One of three experiments is shown. (L) Dextran uptake in basal media was determined by flow cytometry. $n = 3$ /group, one of three experiments is shown. Data represent mean \pm SD. * $P < 0.06$; ns = not significant; one-way ANOVA. (M) Ovarc8, Ovarc3, and Ovarc10 cells were treated with the ATM inhibitor KU60019 (10 μ M) for 2 h in basal media. Immunoblot analysis of p-Chk2 and total Chk2. β -actin was used as a loading control. One of three experiments is shown.

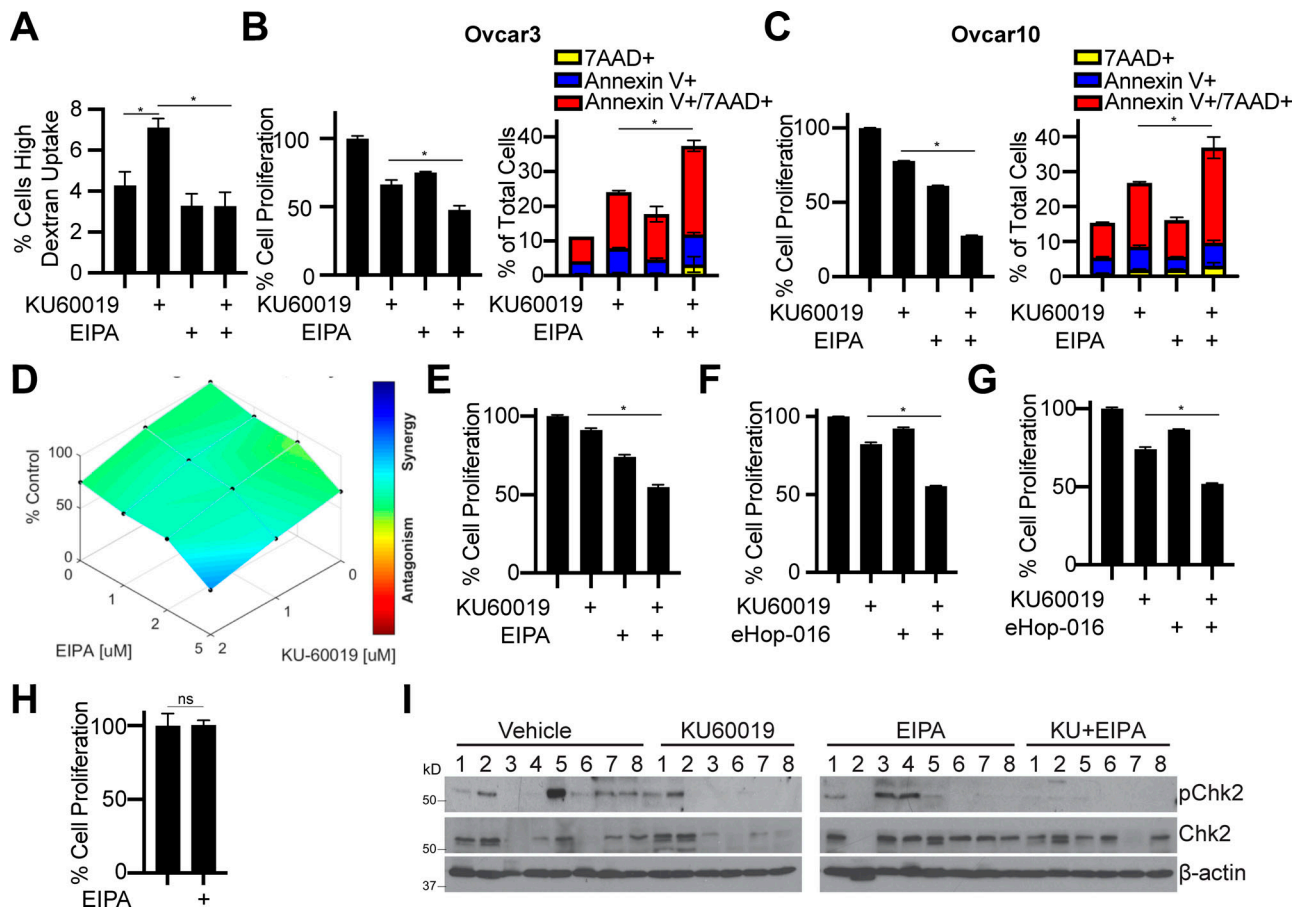


Figure S3. **Inhibition of macropinocytosis inhibits cell proliferation and increases cell death in ATM inhibitor-treated cells.** Related to Fig. 3. **(A)** Ovar8 cells were treated with the ATM inhibitor KU60019 (2 μ M) or the macropinocytosis inhibitor EIPA (2 μ M) alone and in combination for 3 d in RPMI-1640 + 5% FBS complete media, and dextran uptake was determined at the end of the experiment. $n = 3$ /group, one of two experiments is shown. Data represent mean \pm SD. * $P < 0.05$; one-way ANOVA. **(B and C)** Ovar3 (B) or Ovar10 (C) cells were treated with the ATM inhibitor KU60019 (2 μ M) or the macropinocytosis inhibitor EIPA (2 μ M) alone and in combination for 3 d in RPMI-1640 + 5% FBS complete media. Proliferation (left panel) was assessed by crystal violet staining. Apoptosis (right panel) was assessed by Annexin V/7AAD staining. $n = 3$ /group, one of three experiments is shown. Data represent mean \pm SD. * $P < 0.01$; one-way ANOVA. **(D)** Synergy analysis using Combenefit software using the LOEWE model. **(E)** Ovar8 cells were treated with the ATM inhibitor KU60019 (2 μ M) or the macropinocytosis inhibitor EIPA (1.25 μ M) alone and in combination for 3 d in RPMI-1640 + 0.1% FBS complete media. $n = 3$ /group, one of four experiments is shown. Data represent mean \pm SD. * $P < 0.005$; one-way ANOVA. **(F)** Ovar8 cells were treated with the ATM inhibitor KU60019 (2 μ M) or the Rac1 inhibitor eHop-016 (1.75 μ M) alone and in combination for 3 d in RPMI-1640 + 5% FBS complete media. Proliferation was assessed by crystal violet staining. One of four experiments is shown. Data represent mean \pm SD. * $P < 0.001$; one-way ANOVA. **(G)** Ovar8 cells were treated with the ATM inhibitor KU60019 (2 μ M) or the Rac1 inhibitor eHop-016 (1.4 μ M) alone and in combination for 2 d in RPMI-1640 + 0.1% FBS complete media. Proliferation was assessed by crystal violet staining. One of two experiments is shown. Data represent mean \pm SD. * $P < 0.0001$; one-way ANOVA. **(H)** IMR90 fibroblasts (non-macropinocytotic) were treated with the macropinocytosis inhibitor EIPA (2 μ M) for 3 d. Proliferation was assessed by crystal violet staining. Data represent mean \pm SD. ns = not significant. Unpaired two-sided t test. One of two experiments is shown. **(I)** pChk2 and total Chk2 immunoblot analysis in all of the tumors. β -Actin was used as a loading control.

Downloaded from <http://rupress.org/jcb/article-pdf/222/1/e202007026> by Temple University user on 17 April 2024

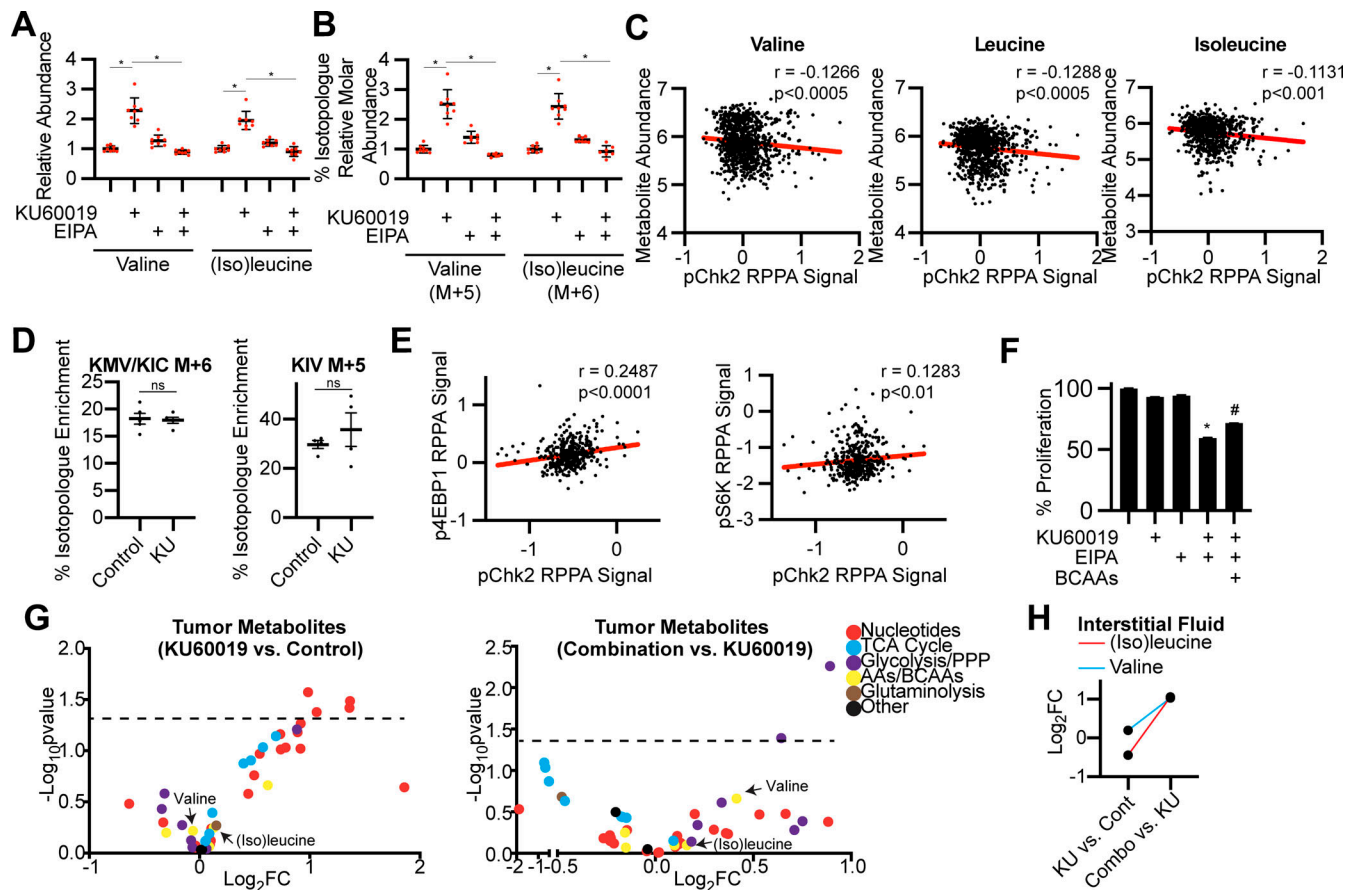


Figure S4. pChk2 protein expression negatively correlates with branched chain amino acids and positively correlates with mTORC1 activity; no change in alpha-ketoacids in ATM inhibited cells; tumor and interstitial fluid metabolites. Related to Fig. 4. **(A and B)** Ovarc8 cells were treated with the ATM inhibitor KU60019 (10 μ M) alone or in combination with the macropinocytosis inhibitor EIPA (25 μ M) for 2 h in basal media. **(A)** BCAA abundance was assessed by mass spectrometry. $n = 8$ /group, one of at least three experiments is shown. Data represent mean \pm SD. * $P < 0.05$ vs. KU60019; one-way ANOVA with Tukey's multiple comparisons. **(B)** Relative percent isotopolog molar abundance (% isotopolog enrichment \times total molar pool size). $n = 8$ /group, one of three experiments is shown. Data represent mean \pm SD. * $P < 0.05$ vs. KU60019; one-way ANOVA with Tukey's multiple comparisons. **(C)** BCAAs metabolite abundance vs. pChk2 protein expression from depmap.org. **(D)** Ovarc8 cells were treated with the ATM inhibitor KU60019 (10 μ M) for 2 h, and isotopolog enrichment of downstream BCAA metabolites (KMV/KIC, KIV) was assessed by mass spectrometry. $n = 3$ /group, one of at least three experiments is shown. Data represent mean \pm SD. ns = not significant; unpaired two-sided t test. **(E)** p4EBP1 and pS6K protein expression vs. pChk2 protein expression from PanCancer TCGA data. **(F)** Ovarc8 cells were treated with the ATM inhibitor KU60019 (2 μ M) or the macropinocytosis inhibitor EIPA (2 μ M) alone and in combination with and without 200 μ M BCAAs for 3 d in RPMI-1640 + 5% FBS. Proliferation was assessed by crystal violet staining. One of two experiments is shown. Data represent mean \pm SD. * $P < 0.0001$ vs. KU60019 and EIPA alone, # $P < 0.0001$ vs. combination treatment; one-way ANOVA. **(G)** Volcano plot of fold change (Log_2FC) of metabolites in ATM inhibitor KU60019-treated vs. control tumors or combination-treated (KU60019+EIPA) vs. KU60019-treated tumors. Dotted line equals $P = 0.05$. **(H)** Fold change (Log_2FC) of metabolites in the interstitial fluid in the indicated treatment groups.

Provided online are three supplemental tables. Table S1 shows tumor metabolites. Table S2 shows antibodies used in the current studies. Table S3 shows RT-qPCR primers.